FACULTY OF
BIOSCIENCE ENGINEERING

Lettuce growth model to support selection and cultivation on Mars

Number of words: 19864

Glenn Van Herrewege
Student number: 01103813

Promoter: Prof. dr. ir. Kathy Steppe
Tutor: ir. Jonathan Vermeiren

UNIVERSITEIT
GENT

Copyright

Acknowledgements

The journey of working on this thesis has been a rewarding and enriching experience. Even in primary school when presented the opportunity of giving a presentation I would choose a topic concerning biology or outer space. Evidently, during the course of my bioscience engineering, I only focused on one of these two fields. I saw an opportunity of combining both fields of interest during my master thesis and got in touch with Professor K. Steppe who helped me brainstorm and guided me to the topic of Lettuce growth model to support selection and cultivation on Mars; which combined modelling and vegetable production in the context of Mars colonisation. The development of this thesis has not been possible without the support of a lot of people.

First, I would like to thank my promoter, Professor K. Steppe whose expertise helped me find a realistic and relevant topic and who shared my enthusiasm for the topic from the start. Furthermore, I would like to thank my tutor, ir. Jonathan Vermeiren. My tutor provided me with the daily know-how and always went the extra mile by giving me fast feedbacks, even during weekends. I am grateful for having him drive me from Ghent to Antwerp back and forth for every day of measurements.

In addition, I would also like to thank Professor M. Baes for his interesting classes of Astrophysics from space which he made easily accessible for me even though I am not a space sciences student. I am grateful to the people of the Research Station for Vegetable Production such as ir. Isabel Vandevelde and ir. Joris Van Lommel. I would also like to thank the International Association of Agricultural Sciences (IAAS) for a wonderful year in which they gave me the opportunity to organise and host a lecture for plant productions in space.

To close, I want to thank all my friends and family, in particular Matthias Vandemoortele together we survived our thesis year - and my best friend and roommate, Jaron Huysentruyt who shares my fascination for space exploration and has always played a supportive role for all my endeavours.

Glenn Van Herrewege

August 2017

Contents

List of abbreviations and symbols

Abbreviation	Definition
A-Ci	Net assimilation rate to intercellular CO2 concentration curve
IRGA	Infra-red gas analyser
LED	Light emitting diode
LRC	Light response curve
NFT	Nutrient film technique
PAR	Photosynthetically active radiation
PSKW	Research Station for Vegetable Production
RuBP	Ribulose 1,5-bisphosphate
UV	Ultraviolet

Roman symbol	Definition	Unit
$[CO_2]_{ref}$	CO_2 concentration measured in the reference IRGA	µmol CO_2 (µmol air)$^{-1}$
$[CO_2]_{sample}$	CO_2 concentration measured in the sample IRGA	µmol CO_2 (µmol air)$^{-1}$
$[H_2O]_{ref}$	Reference IRGA mole fraction of water vapour	mmol H_2O (mol air)$^{-1}$
$[H_2O]_{sample}$	Sample IRGA mole fraction of water vapour	mmol H_2O (mol air)$^{-1}$
A	Net assimilation rate	µmol CO_2 m^{-2} s^{-1}
A_c	RuBP-saturated rate of CO_2 assimilation	µmol CO_2 m^{-2} s^{-1}
A_j	RuBP-limited CO_2 assimilation rate	µmol CO_2 m^{-2} s^{-1}
A_p	Export-limited CO_2 assimilation rate	µmol CO_2 m^{-2} s^{-1}
$BLCond$	Boundary layer H_2O conductivity	mol H_2O m^{-2} s^{-1}
$C_{comp,25}$	CO_2 compensation point at 25 °C	µbar
$C_{Q10resp}$	Increase in respiration for an increase in temperature by 10 °C	-
$C_{rad,rf}$	Transmission through glass roof	-
C_{bnd}	Boundary layer conductance	m s^{-1}
C_{chl}	Chloroplastic CO_2 partial pressure	mbar
C_i	Intercellular CO_2 concentration	µmol CO_2 (mol air)$^{-1}$
C_k	Light extinction coefficient	-
C_{lard}	Proportionality constant between leaf area and dry matter	m^{-2} kg^{-1}
C_{PAR}	Fraction PAR to total incident radiation	-
C_{respr}	Respiration underground parts plant at 25 °C	s^{-1}

C_{resps}	Respiration aboveground parts plant at 25 °C	s^{-1}
C_{stm}	Stomatal conductance	m s^{-1}
C_{τ}	Fraction of underground mass	-
C_{Γ}	CO_2 compensation point at 20 °C	µbar
C_{ε}	Light use efficiency constant at high CO_2 and no respiration	g J^{-1}
$Cond$	Stomatal H_2O conductivity	mol H_2O m^{-2} s^{-1}
DLI	Daily light integral	mol photons m^{-2} d^{-1}
E	Transpiration rate	mol H_2O m^{-2} s^{-1}
F	Molar air flow rate entering the leaf chamber	µmol air s^{-1}
$g_{bnd,CO2}$	Boundary layer conductance to water vapour	mol H2O m^{-2} s^{-1}
$g_{st,CO2}$	Stomatal conductance to CO2	mol H2O m^{-2} s^{-1}
$g_{st,H2O}$	Stomatal conductance to water vapour	mol H2O m^{-2} s^{-1}
I	PAR light intensity	µmol photons m^{-2} s^{-1}
I_c	Light compensation point	µmol photons m^{-2} s^{-1}
I_s	Saturation light intensity	µmol photons m^{-2} s^{-1}
J	Rate of electrons needed for carbon reduction and oxidation	µmol electrons m^{-2} s^{-1}
O	O_2 partial pressure	mbar
$P_{n,max}$	Maximum net photosynthetic rate	µmol CO_2 m^{-2} s^{-1}
P_n	Net photosynthesis	µmol CO_2 m^{-2} s^{-1}
$PARi$	In-chamber quantum sensor (PAR sensor)	µmol photons m^{-2} s^{-1}
$Photo$	Photosynthetic rate	µmol CO_2 m^{-2} s^{-1}
R_d	Day respiration	µmol CO_2 m^{-2} s^{-1}
R_d	Dark respiration	µmol CO_2 m^{-2} s^{-1}
S	Leaf surface area	cm^{-2}
$V_{c,max}$	Maximum carboxylation rate	µmol CO_2 m^{-2} s^{-1}
V_i	Radiation	W m^{-2}
V_{LED}	LED radiation	W m^{-2}
X_c	CO_2 concentration	kg m^{-3}
X_d	Dry matter	g m^{-2}
X_T	Temperature	°C
Γ_*	CO_2 compensation point at 25 °C	µbar

Greek symbol	Definition	Unit
α_c	quantum yield at light compensation point	µmol photons (µmol CO_2)$^{-1}$
α_{gl}	Fraction of glycolate carbon not returned to chloroplast	-
Γ	CO_2 compensation point	ppm
ε	Light use efficiency	g J^{-1}
σ_{CO2}	Canopy conductance for CO_2 diffusion from the ambient air to the chloroplast	m s^{-1}
σ_{car}	Carboxylation conductance	m s^{-1}
$\Phi_{phot,max}$	Maximum response of canopy photosynthesis	g m^{-2} s^{-1}
Φ_{phot}	Response of canopy photosynthesis	g m^{-2} s^{-1}
Φ_{resp}	Respiration	g m^{-2} s^{-1}

Abstract

With the prospect of long duration missions to Mars in the 2030s, there is a need for extra-terrestrial food production. Since transportation of resources into space is an extremely expensive operation, an elaborate screening process designed to carefully select plant species for extra-terrestrial agriculture is important. There are over 100 edible lettuce varieties each with different morphological and physiological characteristics. How do we know which lettuce, tomato or carrot varieties would be most suited for fast production of biomass under the complete controlled environment of a Martian greenhouse? The fastest and most economical way would be to develop models to simulate the growth of the lettuce varieties. This won't only be helpful for evaluating the performance of certain vegetable varieties under specific climatic conditions, but also for predicting the eventual harvest mass of a vegetable.

Three models with different complexities have been developed to predict the dry mass. A simple model based on a simple carbon balance made up out of photosynthesis and respiration and that only uses plant specific parameters. A more complex model based on the model developed by Van Henten (1994) that takes both plant specific parameters and environmental parameters into account. The environmental parameters were temperature, CO_2 concentration, radiation and LED radiation in function of time. The third model was the same as the second model but expanded to be able to work with dynamic plant specific parameters through time. The data to run and calibrate the models have been collected during photosynthesis measurements on different lettuce varieties. Through LRC and A-Ci analysis different plant specific parameters were determined.

The models were able to simulate the growth of the individual lettuce varieties. The simple model based on the carbon balance gave the best fit but was least useable for extrapolation because of its exponential character. Models 2 and 3 had a more realistic growth curve but tended to over- and underestimate the measured masses more. The models were not always able to predict the harvest mass by only using plant specific parameters and environmental data but this could be improved by training the models with more accurate photosynthesis measurement data.

Samenvatting

Met oog op langdurige missies naar Mars in de jaren 2030 is er een nood aan buitenaardse voedselproductiesystemen. Gezien het transport van grondstoffen naar de ruimte een zeer hoge kost met zich meebrengt is een uitgebreide screening van verschillende groenten essentieel. Er zijn meer dan 100 eetbare slavariëteiten beschikbaar met elk hun eigen morfologische en fysiologische eigenschappen. Hoe weten we welke soort sla, tomaten of wortels het meest geschikt zijn om te groeien in de omstandigheden van een groeiruimte op Mars? De snelste en goedkoopste manier zou het ontwikkelen zijn van modellen die in staat zijn de groei te simuleren van individuele groentevariëteiten. Dit zou niet enkel handig zijn voor het evalueren van de productie van bepaalde groentevariëteiten onder specifieke omgevingsomstandigheden, maar ook voor het voorspellen van het uiteindelijke oogstgewicht.

Drie modellen met verschillende complexiteit werden ontwikkeld om de groei te voorspellen in termen van droge massa. Het eerste model was gebaseerd op een eenvoudige koolstofbalans die de fotosynthese en respiratie in rekening bracht. Het gebruikte enkel plant-specifieke parameters. Het tweede model was meer complex en gebaseerd op het model ontwikkeld door Van Henten. Het bracht zowel plant-specifieke parameters als omgevingsparameters in rekening. Deze omgevingsparameters waren temperatuur, CO_2 concentratie, zonnestraling en ledinstraling in functie van de tijd. Het derde model was gelijkaardig aan het tweede maar uitgebreid voor het kunnen werken met plant-specifieke parameters die varieerden in de tijd. De data om de modellen te kunnen kalibreren en uitvoeren was verzameld tijdens fotosynthesemetingen op verschillende slavariëteiten. Plant-specifieke parameters werden berekend door het gebruik van LRC en A-Ci analyses.

De modellen waren in staat de groei van de individuele slavariëteiten te simuleren. Het simpel model gebaseerd op de koolstofbalans gaf de beste fit aan de werkelijke data maar was het minst bruikbaar voor extrapolatie door zijn exponentieel en dus onstabiel karakter. Modellen 2 en 3 hadden een meer realistisch groeiverloop maar hadden de neiging tot over- of onderschatten van de werkelijke data. De modellen waren niet altijd in staat het oogstgewicht te voorspellen met enkel plant specifieke parameters en omgevingsdata maar dit zou verbeterd kunnen worden in toekomstig onderzoek door het gebruik van meer en accuratere fotosynthesemetingen.

Chapter 1
Introduction

Ever since the first space exploration missions in the 1950's led by the Soviet Union and the USA, the focus of space sciences has predominantly been on transport, the physics and machines that get us from Earth to orbit, the Moon or Mars. Afterwards, the sciences of keeping the astronauts alive started to develop. This includes life support systems as we know it on the ISS, but later on also on the production of food on the Moon or Mars.

Space travel is extremely expensive which makes it hard to bring a lot of resources such as food into space. That is why an elaborate screening process designed to carefully select plant species for extra-terrestrial agriculture is of the utmost importance. But most vegetable species have a large number of varieties. Lettuce (*Lactuca sativa* L.) has at least over 100 edible varieties (van Oers, 2017) which makes distinguishing the best variety of the utmost importance. This selection is based on multiple criteria most notably nutritional value, water and energy usage, and time before harvest. This thesis will propose a screening method based on plant physiological parameters of lettuce plants. Since solar radiation on Mars is very low and weather conditions harsh, plants will have to be cultivated in special greenhouses under mostly artificial light.

This research will attempt to construct models that are able to simulate the growth of different vegetables. Different mechanistic models will be assessed for their accuracy and for their ability to distinguish fast growing vegetables from slow growing vegetables. In this case, the experiments will be performed on different lettuce varieties. The models will take climatic factors into account such as temperature, CO_2 concentration and both natural and assimilation light. This assimilation light will be provided by light-emitting diodes (LEDs).

These models could help us decide which vegetable varieties would be economically more interesting to bring to Mars. Not only would such a screening method be applicable for extra-terrestrial applications, but also for horticulture in temperate areas on Earth. With this technique, the right species of lettuce and other vegetables can be selected for growing crops under assimilation light and thus increasing productivities. Being able to grow more vegetables in temperate areas such as Western Europe would fit in the trend towards more local production.

Chapter 2
Literature review

1 Context and progress of space colonisation

Considering extra-terrestrial settlements, the large players in space travel are focussed on the International Space Station (ISS), the Moon, and Mars. While the space agencies of Russia (Roscosmos), China (CNSA) and Japan (JAXA) have shown interest in lunar bases, the agencies of the USA (NASA), Europe (ESA) and private companies have shown interest in Martian bases. Within a matter of decennia, these colonies will arise and with it, the need for plant based life support systems.

1.1 The International Space Station and the Moon

The ISS has been considered as a stepping stone to beyond Earth orbit permanent settlements. It is, at this moment, the only permanently manned spacecraft, and is being used to teach astronauts how to live and work in space. The ISS is the result of cooperation between 5 major space agencies: NASA (United States of America), ESA (Europe), JAXA (Japan), Roscosmos (Russia) and CSA (Canada) (European Space Agency, 2013).

The second option for permanent extra-terrestrial settlements are settlements on the moon. The space agencies of Japan, China and Russia focus on the Moon, rather than Mars. JAXA and Mitsubishi Materials have been developing plans for constructing a manned lunar base in the 2030s, for mining and space observatory (Nikkei, 2016). The Chinese are conducting feasibility studies for manned missions to the Moon with 2020, 2025 or 2030 as potential launch dates (Harrington, 2016). Concerning Russia, in 2015, head of Roscosmos Energia announced that Roscosmos was building a spacecraft for sending people to the Moon in 2029 or 2030. A series of test flights will start in 2021 (Grush, 2015).

1.2 Mars

The third option for extra-terrestrial settlements is Mars.

1.2.1 ESA and Mars

ESA had never engaged in visiting other planets and started with Mars by sending the Mars Express in 2003. It contained an orbiter and a lander (Beagle 2). While the Beagle 2 was declared lost after its landing, the Mars Express Orbiter was a success. It is used by ESA for remote-sensing of the atmosphere, surface and subsurface (European Space Agency, 2004). In 2001, ESA had formulated their ambitions for manned

missions to Mars, in the Aurora Program (European Space Agency, 2006). The long term plan includes the following:

- ExoMars, consisting of an unmanned Mars orbiter and lander conducted jointly with the Russian Federal Space agency in 2016 (Figure 1),
- ExoMars rover launch, which would also be conducted jointly with the Russian Federal Space Agency in 2020 (Figure 1),
- Mars Sample Return, which would be a cooperation together with NASA in the mid-2020s,
- and human space missions in the mid-2030s.

Although there were objections from participating nations concerning the feasibility and the timeline, ESA envisioned to send humans to mars in 2033 (Guteri and Kuyas). Nonetheless, the first of four missions – ExoMars – was launched according to schedule. ESA has sent the Trace Gas Orbiter and a Mars lander called Schiaparelli in 2016. This is an important exercise for descent and landing of payload on Mars. It also investigates the Martian environment and whether life ever existed on Mars. Schiaparelli crashed during the landing. In the second part of ExoMars, ESA will be sending a rover to the red planet (European Space Agency, 2016). Both elements of this mission, the Trace Gas Orbiter and its lander from 2016 and the rover for 2020, are shown below in Figure 1.

Figure 1*. Elements of ExoMars programme 2016 and 2020 (source: ESA).*

1.2.2 NASA and Mars

NASA has started its journey to Mars with long duration low-Earth orbit tests on the ISS. This space station has been a testing ground to prove technologies and communication systems for deep space (Daines, 2015). This also includes the cultivation of plants. The next step were robotic missions on Mars. In 2003, NASA sent two Mars rovers, Spirit and Opportunity. While contact with Spirit was lost since 2010, Opportunity is still being used for exploring the Martian surface and searching for traces of water. In 2012, rover Curiosity joined the robotic Mars missions and measures radiation at the Martian surface (Daines, 2015). Their next step will be running missions with the Orion spacecraft, the successor of space shuttles in deep space (Howell, 2016). The Orion spacecraft is a spacecraft that already has had test flights in 2014 and 2016, in which it orbited the Earth two times and safely returned. In 2018 another unmanned Moon fly by is planned, and in 2023, the first manned fly by, with a safe return to earth (Howell, 2016; Kane). Before

visiting Mars with the Orion spacecraft, NASA intends to send a robotic mission to capture an asteroid and redirect it to orbit the Moon. In the 2020s, astronauts aboard the spacecraft will explore the asteroid and bring samples to Earth (Daines, 2015). The first Martian settlers are to arrive in the 2030s, and will start a settlement (Figure 2) that will thrive on solar power, in-situ source utilisation and on-site manufacturing (e.g. 3D printing). A first impression of what the Martian base would look like can be seen in Figure 2, where the habitat module has been rendered.

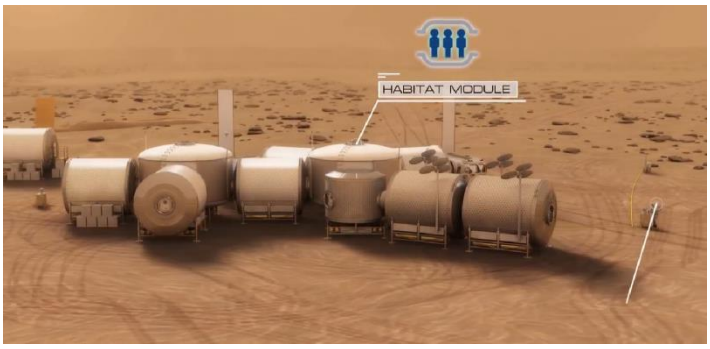

Figure 2. *Habitat module of the envisioned NASA Mars base (source: Space.com).*

1.2.3 Private companies and Mars

Mars One is a Dutch company that aims at building an operating manned Martian base by 2032 (Mars one, 2015a). It will try to land the first 4 people on the red planet with only 6 billion USD. Compared with the 100 billion USD it would cost NASA to start a Martian base, this low cost estimation has received a lot of criticism (Price, 2009). The budget for the operation was estimated so low because it only included a one-way trip and the developers hoped to host a big brother like_reality show, which would cover most of the costs (Wall, 2012). The show would follow the recruiting process, the candidates during the trip to Mars and its first colonization moments. However, after 3 years, in 2015, the reality show got cancelled and replaced by a documentary (Griffiths, 2015).

The selection procedures for the Martian crew started in 2013. The training of the crew will start in 2017. The following years will be used for test flights (2022), sending a rover and communication satellites (2024, 2026) and sending cargo (2029). After the rover has set up the base (Figure 3), the first crews can depart in 2031 and 2033 (Mars one, 2015a).

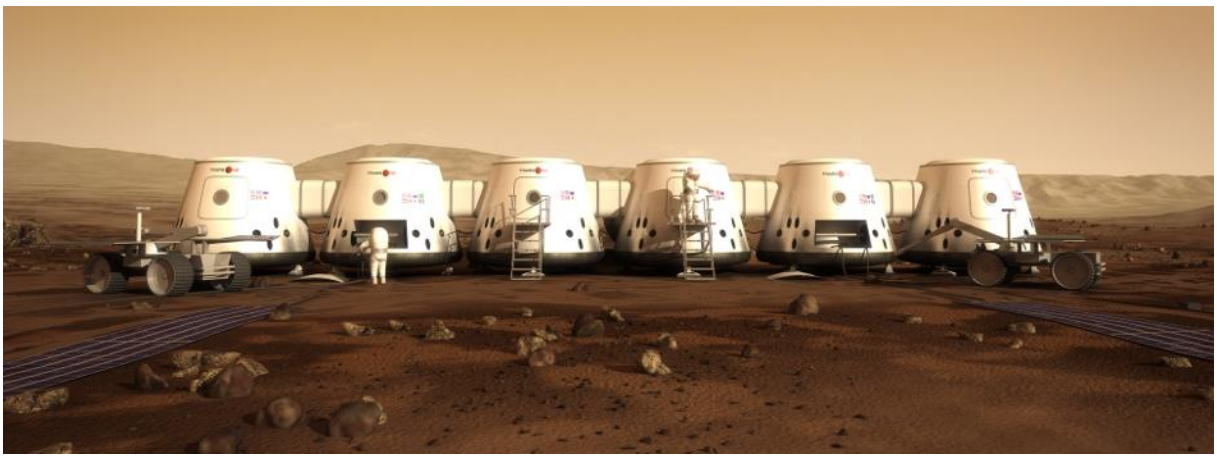

Figure 3*. Render of the proposed Mars One colony (source: Mars One).*

The proposed life support system is called The Environmental Control and Life Support System (ECLSS). Its electricity is powered by thin film solar photovoltaic panels. Water is produced by heating up Martian

soil and separating evaporated water. A part of this water will be used for the production of oxygen. Nitrogen and argon needed for breathable air will be extracted from the Martian atmosphere (Mars one, 2015b).

In order to bring payloads to Mars, Mars One will be working together with SpaceX. The payload can be cargo, rovers, satellites or humans and will be transported using the Space X Falcon Heavy (Mars one, 2015c). Life support systems will be managed by Paragon Space Development (Mars one, 2015d).

SpaceX is a frequently appearing name in the media when it comes to space travel. It is not the aim of this company to colonise Mars but merely to provide the technology to reach the planet. Although it did develop a plan to create a colony for over 1 million inhabitants, it is more involved with the transport systems and less with the life support systems or the colony itself. That is why it has developed rockets such as the Falcon 9, and the Falcon Heavy. For an own proposed colonization method, SpaceX is developing the Interplanetary Transport System (ITS). The ITS includes Mars vehicle rockets. This is a rocket in which the booster returns to earth for reuse (Mars one, 2015d).

2 Habitability of plants on Mars

To evaluate the habitability of plants on other planets, one should first look at major parameters being: temperature, pressure, radiation, chemical composition, gravity and length of day.

2.1 Water

Liquid water on Mars has been found but only as a temporary phenomenon. Since temperatures are too low, water has only been found as brine during warm seasons. This results in slope lineae, or narrow streaks darker than the environment (Ojha et al., 2015). At low altitudes, such as at the bottom of the huge impact crater called Hellas, atmospheric pressure can be double of the planet's surface average resulting in the possibility of liquid water occurring during days when average temperatures exceeds the freezing point of 0 °C (Taylor, 2010). Continuous liquid Martian water is yet to be found, if it exists at all.

Most of Mars' water is contained as ice in the north polar cap. Water vapour often condenses at the surface because of rapid cooling of the thin atmosphere towards nightfall resulting in a thin layer of frost that remains for several hours (Taylor, 2010). Although clouds occur, it likely does not rain on Mars. The clouds occasionally found at the equator consist of water ice. Even if it would be liquid water, precipitation would most likely freeze before reaching the surface (Windows to the universe, 2010). Clouds on Mars can also consist out of condensed CO_2. These only occur in the polar areas during winter and can freeze and precipitate as snow (Taylor, 2010).

It can therefore be concluded that the Martian surface cannot continuously provide liquid water for plant growth.

2.2 Temperature

The temperatures on Mars are too low for plants. Mars has an average temperature of 218.15 K (-55 °C) (Croswell, 2003). At the equator, the surface temperatures can reach as high as 290 K (16.85 °C) during the day, but typically dip down to about 200 K (-73.15 °C) at night (Rapp). The Martian poles cool down during the winter until exactly 147 K (-126.15 °C) since this is the freezing point of CO_2. A further loss of heat would result in more CO_2 deposition on the polar caps (Rapp).

2.3 Pressure

The atmospheric pressure on Mars is too low. It is 6.25% of Earth's atmospheric pressure (6332.8 Pa) (Haeuplik-Meusburger et al., 2014). To be able to grow plants on Mars' surface, at least ~0.1 bar (10 kPa) is needed (Cockell et al., 2016). Plants have adapted poorly to hypobaric conditions. Experiments have shown that a decrease in pressure can cause plants' internal regulatory system to falter. At low pressures, water escapes the plant and causes dehydration, even at 100% relative humidity. This causes the plants to close their stomata (Haeuplik-Meusburger et al., 2014).

Although having such a low pressure, the Martian atmosphere is thick enough to display dynamic phenomena including cloud formation, fronts, storms, and Hadley cells with seasonal variations (Taylor, 2010). Because of the large temperature drop during the polar night, CO_2 condenses and precipitates. This results in two mean surface pressure drops per year. These mean surface pressure drops can be as large as one third of the average surface pressure (Taylor, 2010).

2.4 Radiation

According to Clawson (2005), the daily light integral (DLI) is estimated at 19.4 mol m^{-2} per sol which corresponds to a photosynthetic photon flux (PPF) of 218.9 µmol m^{-2} s^{-1} or 18.91 mol m^{-2} per day or 49.14 W m^{-2}) with one sol being the length of one Martian day or 24 h 37 min 22.7 s. Of this irradiance, 30 % is estimated to be diffuse. An average of 218.9µmol m^{-2} s^{-1} is lower compared to PAR radiation levels on earth. For the month March, a total average of 117.39 W m^{-2} has been measured (Proefstation voor de Groeneteelt, 2016).

Besides PAR radiation, also a large amount of ionising and UV radiation reaches the Martian surface. The magnetosphere of Mars is too weak to maintain a thick atmosphere. Because it is too weak it cannot protect the atmosphere from being blasted away by solar winds (Javaux and Dehant, 2010). The magnetosphere, which is weaker than Earth's, can be explained by the planet's lower mass and the shutdown of its internal dynamo early in its history. Its weakness also results in an inadequate protection against ionizing and UV-radiation (Javaux and Dehant, 2010).

UV is the major liability in short-term exposure to radiation outside the ISS (Tepfer et al., 2012). UV-B radiation outside levels the ISS is too high for plants, inhibiting or reducing photosynthetic processes (Lehto et al., 2006). On Mars, radiation levels are 2.5 times the levels of the ISS, making the situation even worse (Williams; Matt, 2016). Concerning cosmic radiation, only estimated data for human exposure are available. For a person, 600 days on Mars would amount in an exposure of 1 Sievert (Wall, 2013). This is associated with an acceptable 5 % increase in lifetime fatal cancer risk (Wall, 2013). However, in the 18 months the Mars Odyssey probe has been measuring, there have been two solar events in which radiation increased with a factor of 36. Plants would have to be protected against such solar events (Williams; Matt, 2016). A proposed solution would be to bury the plant growth modules under Martian soil.

2.5 Chemical composition

Since the atmospheric pressure on Mars is too low, plants would have to be grown in an artificial and pressurised atmosphere so the chemical composition of the atmosphere becomes less relevant. Furthermore, we know that the Martian soil contains all needed elements for plant production, but not in the right concentrations. The large presence of perchlorates is a major problem. The soil could be made fertile by applying fertiliser and leaching the perchlorates (Cockell et al., 2016; Jordan, 2015).

2.6 Gravity

Martian levels of gravity (0.38 g) are not likely to form a problem for plant growth. Experiments in the ISS with centrifuges indicated attenuation of phototropism in higher plants for gravity less than 0.3 g. The experiment concludes that the gravity on Mars (0.38 g) would probably not form a major problem for plant development. For comparison, this is not the case with the Moon (0.17 g) where its low levels of gravity would affect plant development (Kiss, 2014).

Terrestrial plants withstand the mechanical load of gravity in two strategies (Chebli and Geitmann, 2011). The first one is based on the formation of a hydroskeleton by building a turgor pressure in the plant cells. The second is based on the fortification of the cell wall. This hardening allows plants to stay up straight in the absence of internal turgor pressure. In plants exposed to a change in gravity, one can readily observe a modification in cell wall composition, called gravity resistance (Chebli and Geitmann, 2011). Recent studies by Chebli (2011) indicated that this gravity resistance entails an increased cellulose level in beans. The cellulose levels increased gradually from the apical to the basal regions of the epicotyl which indicates that cellulose functions as a gravity resistance polysaccharide in supporting regions of the seedlings. Besides a change in cellulose levels, hypergravity also affect the orientation of cellulose microfibrils, which in its turn influence the mechanical properties of the cell (Hoson and Wakabayashi, 2015). In the case of microgravity, elongation of *Arabidopsis* hypocotyls and rice coleoptyls were observed. The cell wall rigidity was lower than the controls on earth. The cell walls of the plants under microgravity would have a lower level of cellulose and matrix polysaccharides, suggesting that microgravity reduces cell wall thickness. Also a lower molecular mass in matrix polysaccharides has been observed in *Arabidopsis*. This would be a consequence of an increased activity of the enzymes that break of *Arabidopsis'* matrix polysaccharides. This supports the hypothesis that under microgravity cell walls are less rigid because of an increased cell wall metabolic turnover (Hoson and Wakabayashi, 2015).

2.7 Rotation period

The rotation period of Mars corresponds closely to Earth. It is 1.029 relative to Earth's rotation period. The solar day of Mars, being 24h 37min 22.7 s is also called a sol. Having a lower planetary rotation results in more extreme temperature differences between day and night (Javaux and Dehant, 2010).

2.8 Conclusion habitability plants on Mars

It is clear that plants cannot grow unprotected on Mars. It is too cold, the atmospheric pressure is too low, and there is too much radiation and no continuously liquid water, which makes the planet's surface inhabitable for plants (Figure 4). That is why production of plants is needed with a controlled atmospheric pressure and enough radiation control through ceramic shielding or burying of the module. This protection would leave almost no room for natural light to reach the plants, which is why artificial lighting is essential.

Figure 4. The dry, inhabitable surface of planet Mars. Image taken by Mars rover Curiosity in 2015. (source: NASA, 2015).

3 Growing vegetables

3.1 Growing vegetables on Earth

In areas with restricted sunlight, such as in temperate regions or cities, sunlight can be compensated with artificial lighting. There are different growth lamps available (fluorescent, metal halide, high-pressure sodium and LED) to help with the plant's photosynthetic needs (Monje et al., 2003).

3.1.1 Spectral needs of plants

To produce biomass and regulate growth, a plant needs light of different energy content. The wavelengths with primary importance are ultraviolet (UV), visible light, and infrared (IR). Each wavelength has a different effect on the growth of the plant. Blue light is beneficial for good foliage growth while red stimulates flowering and fruiting. Both are needed for a normal growth and form (Danila and Lucache, 2016).

The primary use of light for a plant is photosynthesis. The wavelengths of the photosynthetically active radiation (PAR) lies between 400 nm and 700 nm (Blindeman et al., 2015). When photons of these wavelength are absorbed by chlorophyll, its electrons become excited, moving to a higher energy state. The excited electrons are transferred through multiple steps that result in the production of ATP and NADPH. These molecules are used to fixate CO_2 into larger carbohydrate molecules. In the meantime chlorophyll, that lost an electron, extracts an electron from water and oxygen is formed during this process (Danila and Lucache, 2016). Since photosynthesis is driven by the number of photons, PAR is expressed in number of photons per second and not as a direct measure of energy although certain wavelengths absorb better than others. The pigment vital for photosynthesis, chlorophyll is a mixture of chlorophyll a and b. Chlorophyll a, which is present in all plants, absorbs light with wavelengths between 430 and 662 nm corresponding to the blue-violet and red spectrum. Chlorophyll b absorbs light with wavelengths between 453 and 642 nm, which is blue and orange related. Carotenoids are other pigments that are red, yellow and orange. Amongst the carotenoids are strong antioxidants which interact with free radicals. Important carotenoids are molecules such as lycopene, alpha-carotene, beta-carotene and lutein. They are synthesised with light waves between 449-475 nm, which corresponds to green and blue spectrums (Danila and Lucache, 2016). These absorption spectra are illustrated in Figure 5.

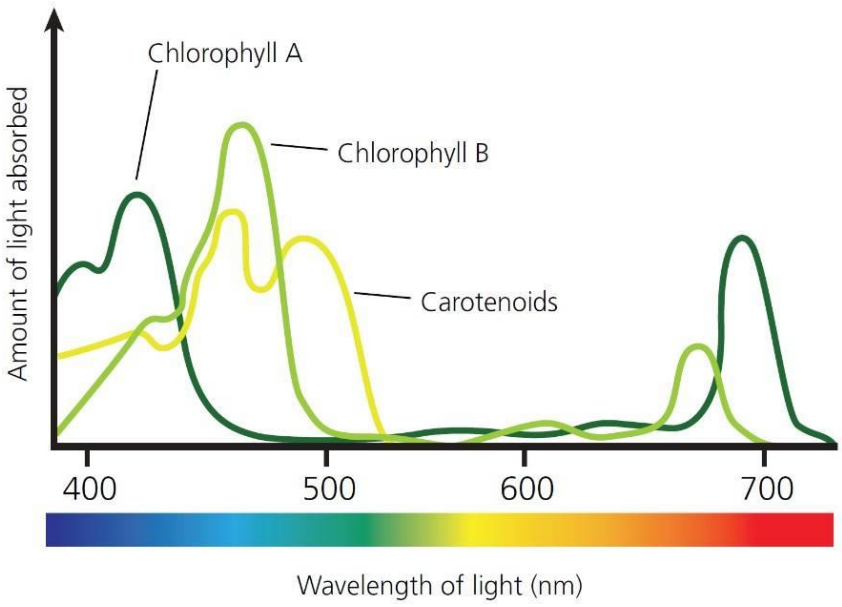

Figure 5. *The absorption spectra of chlorophyll and carotenoids (source: Heliospectra).*

To regulate its photomorphogenesis, light of different wavelengths is essential to plants. That is why lighting systems need to take this into account (Danila and Lucache, 2016).

- Red light stimulates flowering and fruit formation. Phytochrome pigments in plants absorb red photons and regulate seed germination, root development, tuber and bulb formation. It redirects plants from shadow to light. Red light absorbed by most plants has a wavelength between 650 – 680 nm (red to orange).
- Blue light has a larger chlorophyll production stimulating effect than any other colour. It influences the composition and density of the leaves and stimulates a compact vegetative system. Blue light consists out of radiation with wavelengths between 400 and 480 nm. An excess of predominantly blue light favours algal blooms. Young plants tend to need more blue light than mature plants.
- Orange light favours the creation of carotenoids.
- Green and yellow light provide little to no benefits to growing plants.
- Green light is mostly reflected but also tends to penetrate deeper into the canopy since it is less absorbed. This gives leaves deeper within the canopy more photons for photosynthesis even though it is used with a lower efficiency (Danila and Lucache, 2016; Ouzounis et al., 2015).

Furthermore, also the amount of light received is important. The minimum requirement for light is the amount at the light compensation point. This is the minimum amount of light to compensate for respiration (Blindeman et al., 2015). To take both day and night into consideration, one must look at the total sum of light during one day. This is called the daily light integral (DLI) and can be calculated using eq. 1. The DLI determines the growth of the plant. The monthly average DLI of plants in a greenhouse with 70 % light transmission in Belgium varies between about 5 mol m^{-2} d^{-1} in January and December to around 30 mol m^{-2} d^{-1} in June (Blindeman et al., 2015). Converting a light intensity expressed in µmol m^{-2} s^{-1} to a DLI can easily be done by the formula:

$$DLI\ (mol\ m^{-2}\ d^{-1}) = \frac{intensity\ (\mu mol\ m^{-2}\ s^{-1}) \cdot 86400\ s\ d^{-1}}{1000000} \qquad \text{eq. 1}$$

Using this formula, one also has to consider multiplying the value of the DLI with 0.7 as a factor for the transmission through the greenhouse glass if relevant and by 0.5 if the intensity is solar radiation, since only 50 % of solar radiation is PAR.

In addition, the duration of light exposure is equally important. The length of day incites a plant to start blooming, sprouting or start a dormant phase. This concept of photoperiodicity can actively be used in horticulture. Since plants measure the day length by the hours of darkness, nights can be interrupted by using lamps for 2 to 4 hours with low light intensities (2 µmol m^{-2} s^{-1} and higher) (Blindeman et al., 2015).

3.1.2 LEDs and varying spectrum distribution

Studies performed by Massa et al. (2008) have indicated that plants receiving only red light are more likely to develop deformities and grow poorly, while when adding percentages of blue light, plants grow normally. Experiments with *Arabidopsis*, lettuce and soybean showed that a minimum of 15-30 µmol m^{-2} s^{-1} of blue light is needed for a normal morphology (Avercheva et al., 2016; Hoenecke et al., 1992). The same experiments performed by Massa et al. indicated that plants under white light still performed better in dry weight production than plants grown under red and blue LEDs (Massa et al., 2008). Although this seems to be correct for plants such as radish and spinach (Massa et al., 2008; Yorio et al., 2001), other plants such as lettuce and wheat seem to outperform their white light control plants with only red and blue light (Yorio et al., 2001).

3.1.3 Lighting Systems for Greenhouses

In this part, an attempt will be made at clearing out the types of lamps and what exactly makes them different. Figure 6 compares the different light spectra of these lamps. In Figure 6, also green and yellow light can be seen for LED light. LEDs produce light at a specific wavelengths, usually 95% red and 5% blue LEDS. In this case also yellow and green LEDS were used.

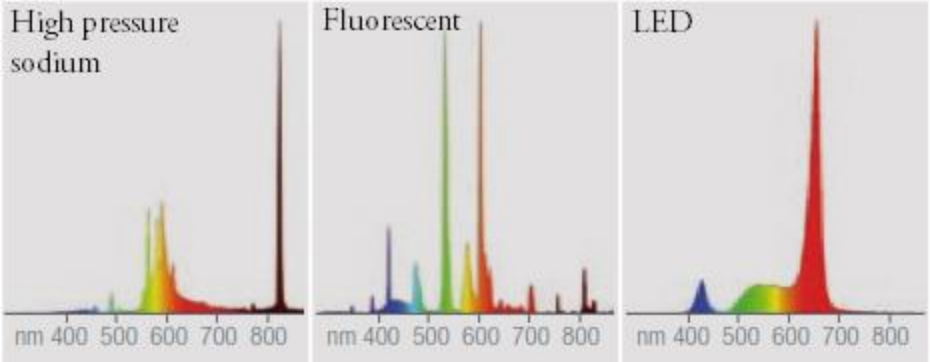

***Figure 6**. Comparison of various colour spectra for high pressure sodium lamps, fluorescent lamps and LEDs* (Blindeman et al., 2015).

3.1.3.1 Fluorescent lamps

Fluorescent lamps (Figure 7) used to be the most popular type of grow lamps (Resh, 2013). They consist of a phosphor-coated glass tube containing small amounts of mercury and inert gases. A cathode creates an arc which vaporises the mercury, which in its turn generates UV-light. The UV-light reacts with the phosphorous coating to generate visible light (Cole and Driscoll, 2014).

Two widely used fluorescent lamps for growth are the tube-style fluorescent light and compact fluorescent light. Tube-style fluorescent lamps need a special fitting, have an average lifespan of 20 000 hours and produce 33 to 100 lumens W^{-1} (Reed and Canadian Electronic Library, 2011). Compact fluorescent lamps fit in a standard lamp fitting, have an average lifespan of about 10 000 hours and produce 44 to 80 lumens W^{-1} (Ahuja, 1997; Reed and Canadian Electronic Library, 2011). The corresponding spectrum temperatures can be warm (red) (2700 K), daylight (full spectrum) (5000 K) and cool (blue) (6500 K). In addition, red is recommended for flowering, while blue is recommended for vegetative growth (Resh, 2013).

***Figure 7**. Example of a tube-style fluorescent lamp (left) and a compact fluorescent lamp (right) (source: bulbcycle, bhphotovideo).*

3.1.3.2 High intensity discharge lamps

High intensity discharge lamps (Figure 8) are currently the most popular grow lights available. They also produce light by running current through a gas, but unlike fluorescent lamps, no phosphorous layer is needed to produce visible light. The first high intensity discharge lamps were mercury vapour lamps. Although this technology was a major advancement in terms of efficacy (lumen W^{-1}), it suffered from a major depreciation after the published 24 000 h lifespan. This resulted in users reluctant of replacing old but working lamps. High intensity discharge lamps entail a whole family of lamps, such as metal halide, high pressure sodium and low pressure sodium (Cole and Driscoll, 2014).

The first type of high intensity discharge lamps is the metal halide lamp. Metal halide lamps or multi-vapour lamps include other compounds to increase the efficacy and colour rendering significantly. The downside of the increased efficacy was its usable lifespan: 40 % to 60 % less than mercury vapour lamps (Cole and Driscoll, 2014). The lamps emit more in the blue and violet parts of the spectrum, more similar to light during spring (Clarke, 2013). This light is more similar to sunlight than other high intensity discharge lamps such as the high pressure sodium (HPS) lamp. High pressure sodium lamps distort the colour of plants more. That is why metal halide lamps are used more for plants displayed at home. Metal halide bulbs need replacement every year, which is only half as long as the average HPS lamp (Zachos) and produce 60 to 125 lumens W^{-1} (Reed and Canadian Electronic Library, 2011).

The second type is the HPS lamp. As the name indicates, the compound added to high pressure sodium lamps is sodium. These lamps give a yellow or golden colour, which is less suitable for plants, but is compensated by its high efficacy and long lifespan. Since these lamps distort colour, they became the popular choice for indoor facilities where colour was not an issue (Cole and Driscoll, 2014). Besides yellow, HPS lamps also produce light in the red part of the spectrum and small portions in the other parts of the visible spectrum. This red light can stimulate blooming and fruiting (Resh, 2013). HPS lamps produce 60 to 140 lumens W^{-1} (Ahuja, 1997). In Belgium, these lamps are often used and are called SON-T lamps. These are high pressure sodium lamps made by Philips.

The third type of high intensity discharge lamps are the low pressure sodium lamps are not used as grow lights. They produce a monochromatic yellow light because of an indium tin oxide coating (Lamptech, 2015) which makes it not suitable for plant production. Its use is limited to roadway applications (Cole and Driscoll, 2014).

***Figure 8**. Examples of a metal halide lamp (left) and high pressure sodium lamps (right) (source: usalight, eyehortilux).*

3.1.3.3 LED

LEDs (Figure 9) are not lamps as we know them. They are electronic devices consisting of thin layers of semiconductors. Layers of indium gallium nitride, which are negatively charged, are sandwiched between layers of gallium nitride, which are positively charged. By changing the composition of the "sandwich" layer material, LEDs can be tuned to emit light of a specific wavelength. LEDs have become more and more popular because of dramatic improvements in a short period of time. Compared to fluorescent and metal halide lamps, LEDs have a higher efficacy and lifespan. This trend of increasing efficacy and lifespan is expected to continue in the coming decennium (Cole and Driscoll, 2014). What makes LEDs valuable is that light can be produced in certain wavelength ranges, making it possible to selectively feed the plant with PAR light. This has a large impact on the electricity consumption of lighting systems. Another advantage is the fact that LEDs produce less heat (Blindeman et al., 2015).

***Figure 9**. Left: an example of a LED lamp used for horticulture. Right: the application of LEDs for lettuce production with arrows indicating the location of the lamps (sources: winlight, Glenn Van Herrewege).*

3.2 Growing vegetables in space

Since 1970, around 50 different plant experiments have been conducted with 21 different plant growth chamber designs in outer space from short durations on the Shuttle (Zabel et al., 2016) to long experiment duration on the space stations. These different plant growing chambers are summed up in Figure 10 and Appendix Figure A1 per space station (Zabel et al., 2016). Plant growth systems are essential for closing different loops in life support systems, which will be needed if we would ever venture into deep space with long flight times or start extra-terrestrial colonies. Its functions are CO_2 reduction, O_2 production, waste recycling and water management. It also has a positive impact on the psychological health of the crew (Zabel et al., 2016).

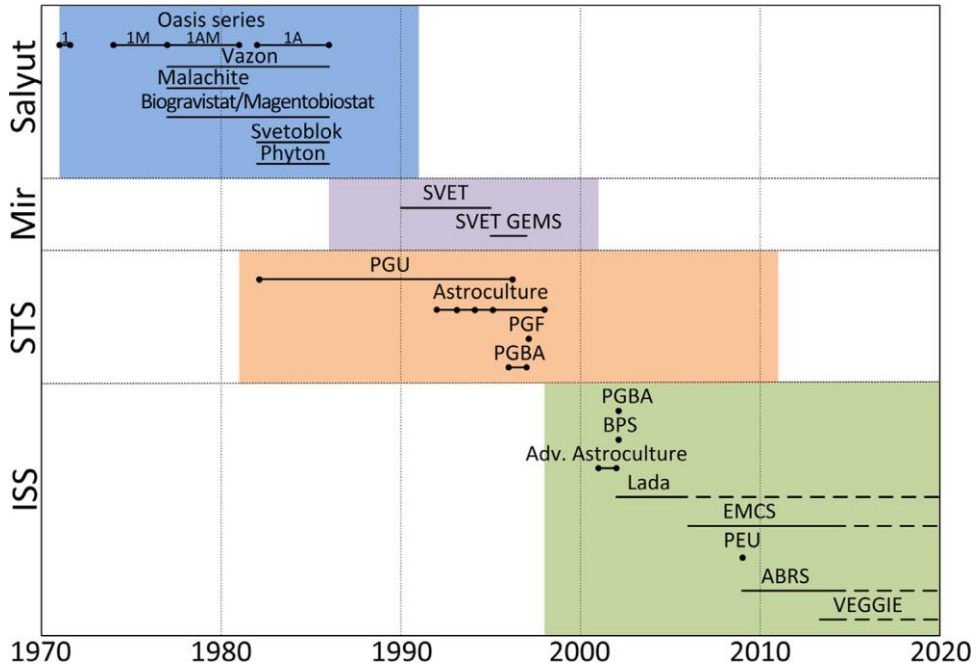

***Figure 10**. Timeline of the different plant growth chambers flown or proposed to fly in space* (Zabel et al., 2016).

3.2.1 Evolution of growth chambers through time

At this moment the experiment called VEGGIE is being conducted on the ISS. In this project, astronauts were allowed by NASA to eat their own grown crops for the first time ever in 2015. The growth chambers changed a lot through the years. Technical innovation takes place on the illumination systems, the atmospheric management systems and the nutrient delivery systems (Zabel et al., 2016).

The development of the illumination system can be divided in a pre-LED era and a LED era. In the pre-LED era, fluorescent and high-pressure sodium lamps were mostly used. After the 2000s, the materials for LEDs became more available and the efficiency improved. The advantages of LEDs were their high efficiency, their small size, their controllability and their variable spectrum. By changing the composition of colours, LEDs are suited for imitating dusk and dawn. Mostly red (~660nm) and blue (~450nm) LEDs were used. There have also been experiments with having wavelengths in the infra-red or green spectral range since this could have an effect on secondary ingredients such as antioxidants and vitamins. The current project (project VEGGIE) also uses green LEDs besides red and blue. An overview of the used illumination systems can be found in the Appendix TableA2 (Zabel et al., 2016).

Furthermore, atmospheric management systems need to be managed. Early systems like the Oasis series and Vazon on the Saylut stations were open systems and cultivated plants in the cabin's atmosphere. The following systems did have atmospheric management systems that controlled the temperature and later also humidity and CO_2 control. Temperature control was needed since the fluorescent lamps produced an excess of heat. CO_2 was controlled by injecting pure CO_2 or in one case by also using CO_2 absorption beds. Since the Advanced Astroculture growth chamber in 2001, some growth chambers also had trace gas control. Usually this would be an ethylene scrubber (Danila and Lucache, 2016). Scrubbing ethylene was important to close the material loop, but also to preserve the fruit longer. Ethylene would be removed or by a scrubber that oxidises ethylene into CO_2 and water or by an ethylene filter. An overview of the used atmospheric management systems can be found in Appendix Table A3 (Zabel et al., 2016).

The largest challenges in plant production in space lay in nutrient delivery. There is no gravity on the ISS to drain the water, which results in difficulties in water movement control or distribution. This often resulted in flooding and anoxia. Several nutrient delivery systems have been tested. These include ion exchange resins in water compartments, the use of agar, perforated tubing, porous tubes and manual water and nutrient supply. Although still facing many challenges, porous tubes and porous plates still promise to be the nutrient delivery system in future on-orbit systems. An overview of the used nutrient delivery systems can be found in Appendix Table A4 (Zabel et al., 2016).

4 Crop Growth Modelling

To be able to predict if certain vegetable species or varieties will have higher production yields, crop growth models can be used. Models that are based on sound physiological data enable us to collect data about new plants or environmental conditions in a small time scale and in a low-cost manner. Models also enable the fast screening of a large number of possibilities. Crop growth models are models based on mathematical equations that represent the physiological processes within the plant and the interactions with its environment. It also takes into consideration the growth of its components, such as the leaves, roots or stems. These models do not only offer information about the total biomass but also deliver valuable quantitative information about the processes that contribute to the total biomass (Gowda et al.).

There are two different types of crop growth models. The first one is empirical or corrective models. This is a black box method in which a relationship is found between different variables without uncovering any underlying physical or biological relations. This type of model uses data to find a mathematical equation to describe the behaviour of a system through, for example, a regression. This is useful when in practice many variables influence the growth of a crop and when it is impossible to quantify all relevant variables through multiple field experiments. The second type are the explanatory models. These models describe the physiological processes that contribute to the behaviour of the plant. Each mechanism is quantified separately and integrated when building the model (Gowda et al.).

A lot of crop growth models are available. Especially for wheat, maize, potato, rice and cotton (Di Paola et al., 2016). The model that will be used as a basis for this thesis will be the Van Henten model for lettuce growth. This model is especially designed and validated for the photosynthetic production of lettuce. The limited other available models for lettuce production are the ones of:

- Seginer *et al.* (2004), called the NICOLET lettuce model. This model has been developed to predict the growth of greenhouse lettuce plants in function of nitrate content. Different versions have been developed for different N-stress levels. What distinguished the NICOLET model are the osmotic balance of the vacuole, the dry carbon compartment and the subdivision of structure into different composition categories (2004). Since the model of this thesis assumes no water or nutrient limitation, these features would only add unnecessary complexity.

- Seginer & Ioslovich (2005), which focusses more on nitrate-limited experiments by including transportation of nitrate from and to the vacuole (Read et al., 2015). For the same reason as for the model of Seginer *et al.* of 2004 this model is less relevant since the model of this thesis assumes no water or nutrient limitation.

- Salomez *et al.* (2007), which has been developed for Flemish greenhouse farmers with butterhead lettuce. The model focusses on two environmental parameters, the soil temperature and the short-wave radiation.

Experiments were followed up during two consecutive years whereby head fresh weight, soil temperature and short-wave radiation were measured (Salomez and Hofman, 2007).

These recent models have known their applications in agricultural practices (Salomez and Hofman, 2007; Seginer et al., 2004) and policy making (Read et al., 2015), but still a preference is given to the model developed by Van Henten in 1994. This model focusses on the dry weight production, which is the eventual aim for selecting vegetables to bring to Mars or grow for high yields. It is a general model with environmental factors as inputs that are easily adaptable to allow plant specific inputs. The simple and versatile structure of this model makes it the best choice as a basis for the models further to come.

Chapter 3
Materials and methods

1 Experimental set-up

Vegetables valuable to bring to Mars are the ones that produce a high usable biomass under specific light, temperature and CO_2 conditions. In order to develop a method for selecting vegetables which are valuable to bring to Mars, the factors which have a significant influence on the growth have to be determined. The amount of factors also has to be taken into consideration as measurements shouldn't be needlessly complex. Influencing factors could be plant specific parameters such as maximum photosynthetic rate and stomatal conductivity for water and CO_2, or climatic parameters such as temperature, CO_2 concentration or incident radiation.

In this thesis, different lettuce varieties were screened for photosynthesis under different microclimatic conditions These include photosynthetic production under changing light conditions in a light response curve (LRC) and values of photosynthetic production under changing CO_2 conditions in an A-C_i curve. This information will be combined with climatic information obtained by the climate computer Synopta (Hortimax, Maasdijk, The Netherlands) and incorporated in a lettuce growth model. The three photosynthetic production models that will be discussed in this section are: 1. a model based only on plant specific parameters, 2. a model based on both plant specific and climatic parameters, and 3. a model based on dynamic plant specific parameters and climatic parameters, as represented in Figure 11.

1.1 Lettuce

1.1.1 Lettuce varieties investigated

The varieties of lettuce investigated originate from the seed companies Rijk Zwaan (De Lier, The Netherlands) and Enza Zaden (Enkhuizen, The Netherlands) and will be grown at the Research Station for Vegetable Production (PSKW, Sint-Katelijne-Waver, Belgium). They were delivered as seedlings in blocks of soil, and placed in a gully system once they were a couple of days or a week old, as seen on. This gully system was the implementation of a nutrient film technique which is a form of hydroponics (Figure 13) (Cook, 2015). The investigated varieties are shown in Table 1 together with their cultivar group, colour and types of experiments performed. The experiments included measurements to create a light response curve (indicated with LRC) or an A-Ci curve (indicate with A-Ci). The investigated lettuce varieties were Mondaï, Saturdaï, Xandra, Fairly, Lucrecia and Presteria. Mondaï, Saturdaï and Xandra are red while Fairly, Lucrecia and Presteria are green lettuce varieties. Xandra, Saturdaï and Mondaï were varieties of oak leaf lettuce while

Fairly, Lucrecia and Presteria are part the butterhead lettuce varieties (Table 1, Figure 12) (Rijk Zwaan; Ryder, 1999).

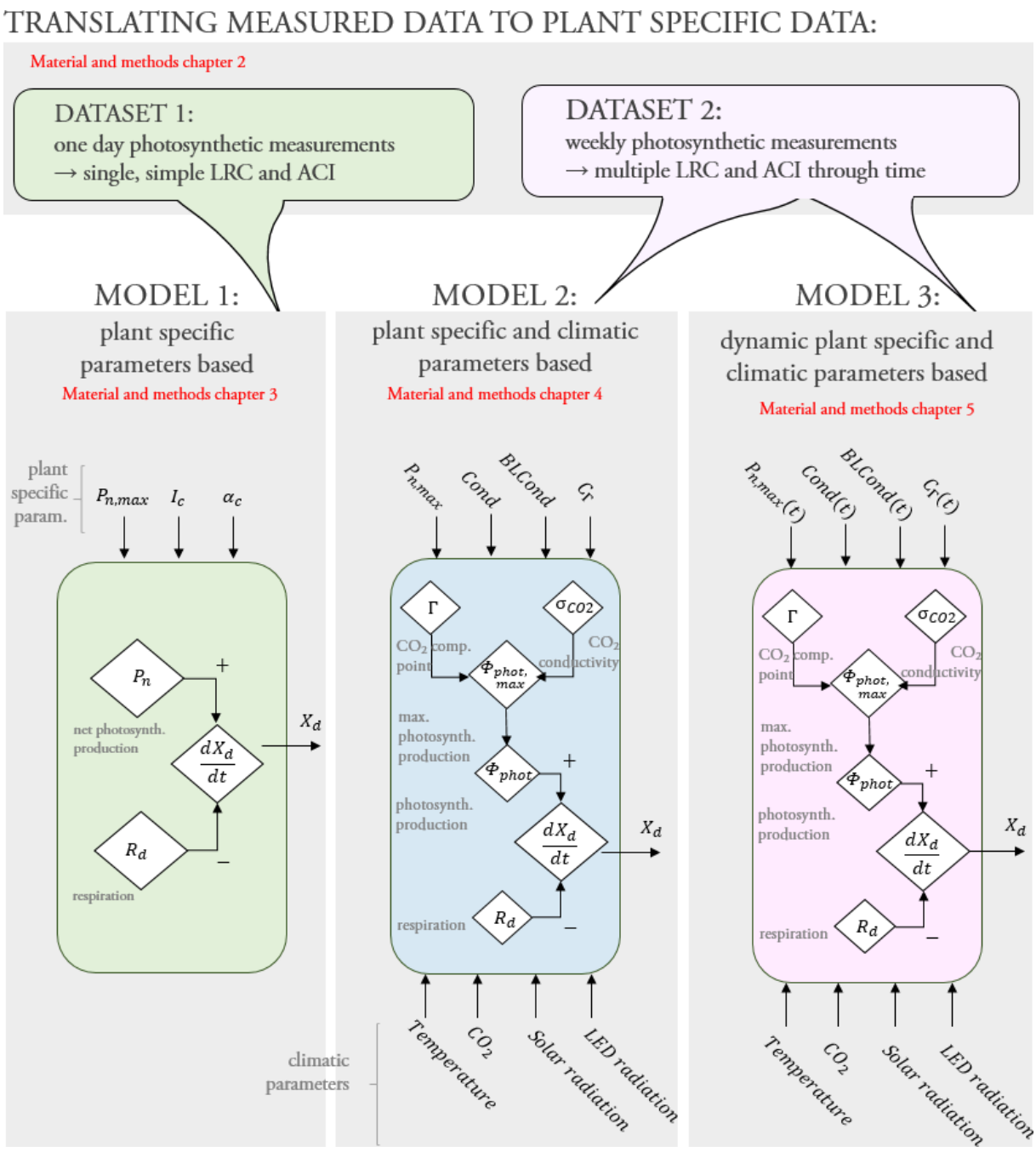

Figure 11. *An overview of structures in the chapters of materials and methods. The differences and similarities between models 1, 2 and 3 can be seen it its inputs and model build-up.*

***Table 1**. The different lettuce varieties on which experiments were performed together with its horticultural group, its colour and the experiments that were conducted. The experiments are indicated by an LRC for a Light Response Curve and an A-Ci for an A-Ci curve together with the number of repetitions for each measurement.*

Cultivar	horticultural group	horticultural subgroup	Vegetable breeding company	Colour	Experiments
Mondaï Saturdaï Xandra	Leaf	Oak leaves (eikenblad-sla)	Rijk Zwaan	Red	Single day measurements LRC (x5) and A-Ci (x5) Weekly measurements LRC (x3 or x4) and A-Ci (x1)
Lucrecia Presteria	Butterhead	Butterhead (kropsla)		Green	Single day measurement LRC (x5) and A-Ci (x5)
Fairly			Enza zaden		

***Figure 12**. (a) Mondaï, oak leaf lettuce, (b) Saturdaï, oak leaf lettuce, (c) Xandra, salanova, (d) Presteria, butterhead lettuce, (e) Fairly, butterhead lettuce, (f) Lucrecia, butterhead lettuce (Rijkzwaan, Enza zaden).*

1.2 Nutrient Film Technique

The lettuce plants were cultivated in a gully system using the nutrient film technique, as seen in Figure 13. This is a technique developed in the late 60's by Dr. Allan Cooper in the UK. It is a hydroponic production method in which a thin film of nutrient solution flows through channels or gullies which contain the plant roots. The root mat or anchoring medium is partly above the shallow stream of recirculating solution to ensure adequate oxygen levels for the root system (Morgan, 1996). Often, no medium or rock wool is used. In this set-up, cubes of soil with a length of 5 and 6 cm were used. The key requirements in achieving a

nutrient film situation are 1) to ensure a uniform water flow, so no local water level depressions can occur, 2) inlet water flow rates must not be too high so that water levels remain shallow, 3) the channel must be wide enough to avoid any damming up of the solution. If this is the case, yields are directly proportional to the channel width. 4) A flat base of the channel is needed to maintain a constant shallow solution layer (Cooper, 1970; Morgan, 1996).

The slope of the channels is also an important factor. A light slope of 1 in 50 to 1 in 75 seemed to be suitable, while a drop of 1 in 100 seemed to be insufficient. In the case of PSKW the slope amounts to 3 %. To avoid anoxic regions in the nutrient solution, immobile solution regions must be avoided by having no depressions in the channel floors. Excessively long channels can cause problems such as differences in nutrients, pH, temperature and oxygen loss. As long as channels remain under 3 meter in length, no such problems can occur. Even so, channel lengths to well over 20 m are being used in practice (Morgan, 1996). In this case, the channel lengths were 11.8m.

The main advantage of this system is the greatly reduced amount of nutrient solution needed. This was important during the winter months since heating of the nutrient solution could be needed to maintain optimal temperatures for growth (Cooper, 1970).

The nutrients that were being added to the circulated water were kept in two separate solutions which were mixed before usage. The A solution contains nitrates and chelated iron, while the B solution contains phosphates, sulphates and trace elements.

***Figure 13**. The gully system in which the lettuce plants were grown for 7 weeks.*

1.3 Portable photosynthesis systems for gas exchange

Photosynthetic measurements were performed using the LI-6400XT (LI-COR Biosciences, Lincoln, NE, USA). The LI-6400XT consists out of a console and a sensor head. The sensor head (Figure 14) can be placed over a leaf to measure its photosynthetic rate. The leaf can be confined inside the leaf chamber where red and blue LEDs emit a controlled amount of light on the leaf which drive photosynthesis. The CO_2 concentration, humidity, temperature and light intensity a measured and controlled within this leaf chamber. The LI-6400XT measures the photosynthetic rate of the enclosed leaf area by measuring its CO_2 uptake with an infra-red gas analyser (IRGA).

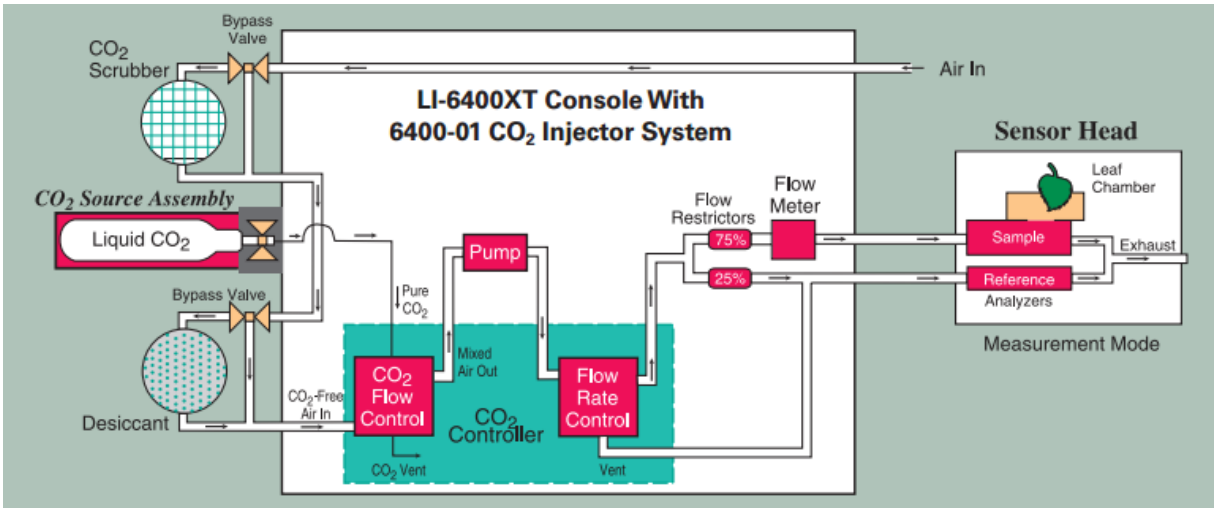

***Figure 14**. Schematic overview of the LI-6400XT (source: LI-COR Biosciences).*

The leaf chamber is an open differential chamber. It is an open system because air with a controlled CO_2 concentration continuously passes through the sensor head via two different routes. The first route passes through the leaf chamber where CO_2 concentrations changes due to leaf photosynthesis and respiration. The second route flows through a reference cell which doesn't contain a leaf. It's a differentiated system because the difference between the CO_2 concentrations in both flows is measured and equals the amount of CO_2 fixated or released due to photosynthesis and respiration. The CO_2 concentration is controlled by the CO_2 mixer in the console. The inlet air is first scrubbed from all CO_2 with a soda lime packed scrubber. Then, a known amount of CO_2 is added to the airflow. The net photosynthesis P_n is then calculated by the LI-6400XT (eq. 2).

$$P_n = \frac{F \cdot ([CO_2]_{ref} - [CO_2]_{sample})}{100 \cdot S} - [CO_2]_{sample} \cdot E \qquad \text{eq. 2}$$

$[CO2]_{ref}$ represents the CO_2 concentration measured in the reference chamber and $[CO_2]_{sample}$ represents the CO_2 concentration measured in the leaf chamber both expressed in µmol CO_2 (µmol air)$^{-1}$. F represents the air flow rate (µmol s^{-1}), S the leaf surface (cm^2), and E the transpiration rate (mol m^{-2} s^{-1}). Transpiration is included as a correction for dilution of CO_2. As the leaf transpires, it adds water vapour to the chamber diluting other gasses. E can also be written in function of $[H_2O]_{ref}$ and $[H_2O]_{sample}$ or the reference and sample water mole fractions, which results in eq. 3.

$$P_n = \frac{F \cdot ([CO_2]_{ref} - [CO_2]_{sample}(\frac{1000 - [H_2O]_{ref}}{1000 - [H_2O]_{sample}}))}{100 \cdot S} \qquad \text{eq. 3}$$

Using the plant modelling software PhytoSim (Phyto-IT, Mariakerke, Belgium), LRCs and A-Ci curves were fit to the data measured with the LI-6400XT, as can be seen in Figure 15.

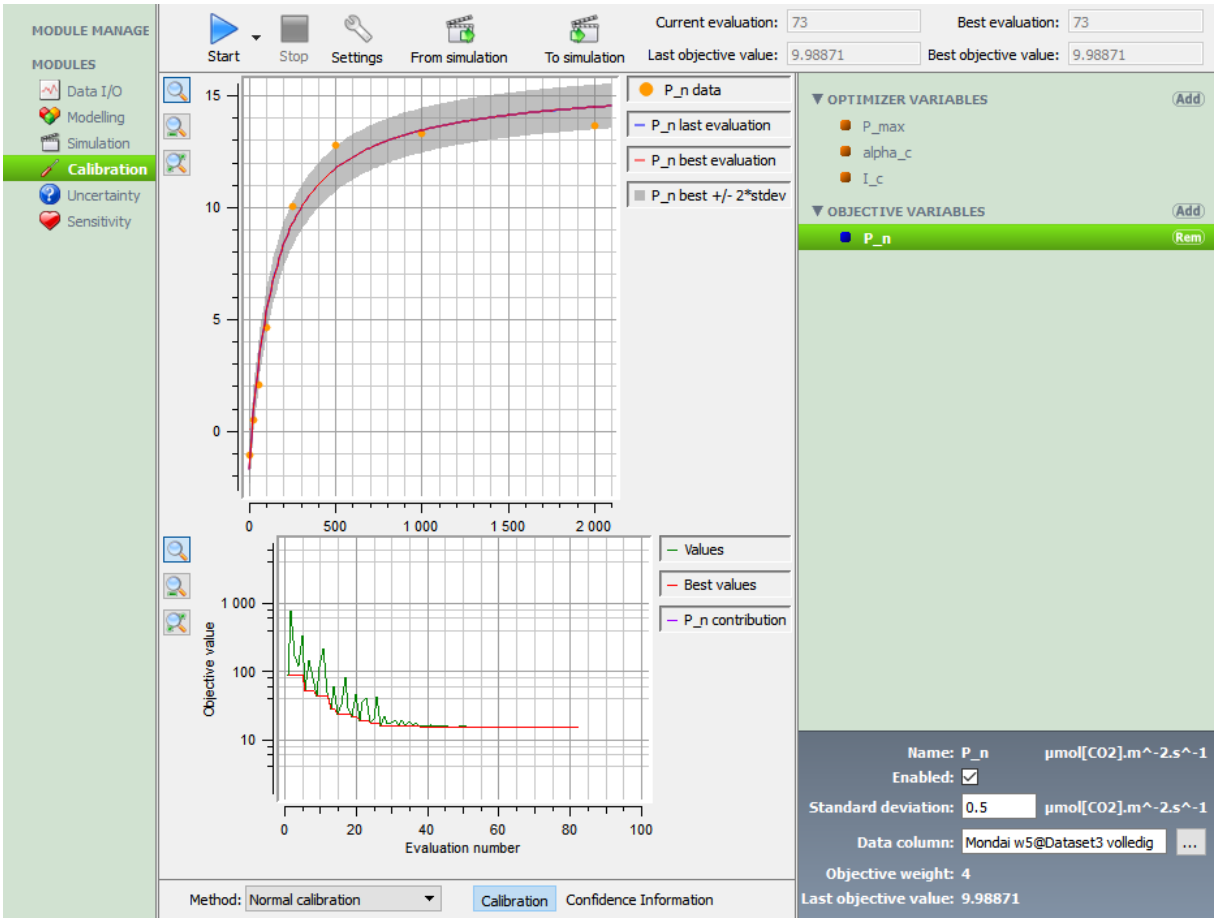

Figure 15. *The interface of PhytoSim during a calibration of an LRC to photosynthetic measurements of Mondaï.*

2 Translating measured data to plant specific parameters

2.1 Introduction

The models to predict the harvest weight of the plants will use the plant growth model developed by Van Henten in 1994 as a basis. To be able to make the models discussed in the next chapters plant specific, a link must be established between the parameters used in the models and the parameters measured by the LI-6400XT. An overview of how these values were translated to inputs for the Van Henten model is represented below in Figure 16. Next sections will elaborate on these different transformations. Photosynthetic measurements were performed by using the Li-6400XT to be able to construct LRCs and A-C_i curves (Figure 18).

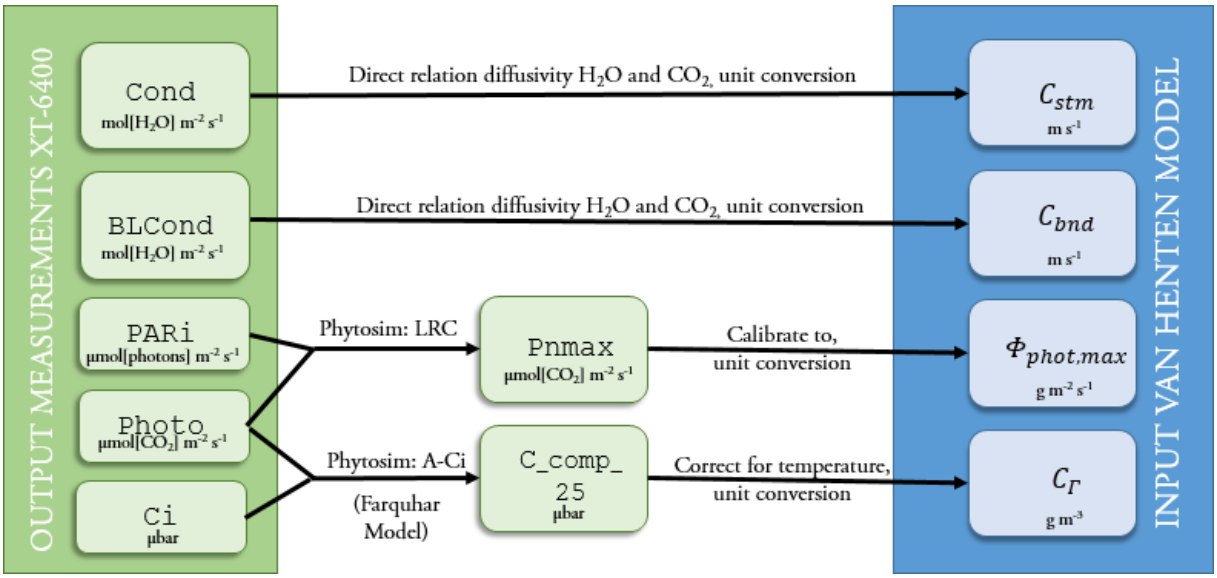

***Figure 16**. Overview of the transformations from plant specific parameters as measured by the LI-6400XT.*

2.2 Light Response Curve

An LRC shows the relation between the photosynthetic rate of a leaf and the light intensity expressed in PAR (µmol photons m^{-2} s^{-1}). Photosynthetic rate was expressed as the amount of CO_2 fixated (µmol CO_2 m^{-2} s^{-1}). The LRC indicates that at low photon fluxes, there is a linear correlation between the light intensity and the CO_2 assimilation (Figure 17). At higher photon fluxes the photosynthetic rate stagnates. From this curve five parameters could be derived:

- $P_{n,\max}$ or the maximum net photosynthetic rate (µmol CO_2 m^{-2} s^{-1}). $P_{n,max}$ is computed from LRC measurements reaching up to 2000 µmol PAR m^{-2} s^{-1} and at 550 ppm CO_2 .
- α_c or the quantum yield at light compensation point (µmol photons (µmol CO_2)$^{-1}$). It expresses how many moles of photons are needed to fixate one mole of CO_2 at the light compensation point.
- R_d or dark respiration (µmol CO_2 m^{-2} s^{-1}). It indicates the metabolic activity of a plant.
- I_c or the light compensation point (µmol photons m^{-2} s^{-1}), which is the intensity where the photosynthetic production rate compensates the respiration rate .
- I_s or the saturation light intensity (µmol photons m^{-2} s^{-1}). At radiation levels higher than the I_s, the photosynthetic production rate doesn't increase any further.

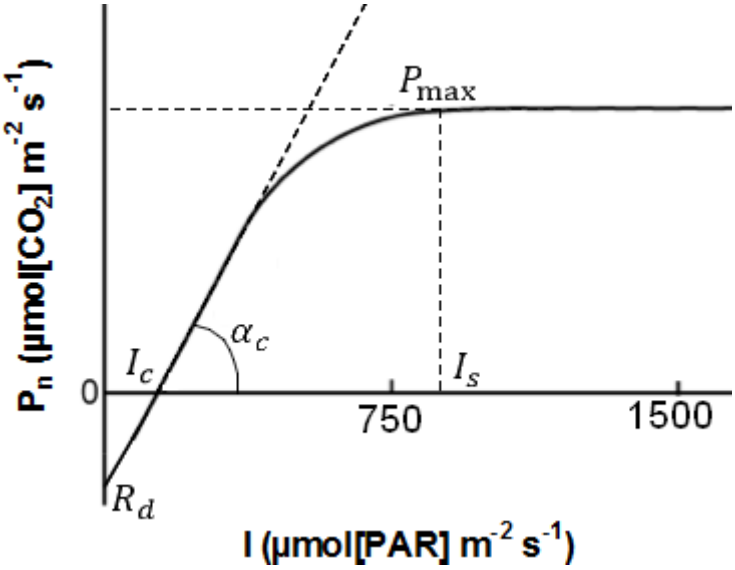

Figure 17*. An example of a light response curve with its 5 important parameters.*

These parameters can be derived manually through the Method of Drake, but since this is only an approximation, preference was given to computing these parameters using PhytoSim. The three parameters (P_{max}, I_c and α_c) were optimised in order to fit the model (eq. 4) to the data.

$$P_n = P_{n,\max} \cdot \alpha_c \cdot \frac{-I_c}{P_{\max} + \alpha_c \cdot (I - I_c)} \qquad \text{eq. 4}$$

I represents the PAR light intensity in µmol photons m^{-2} s^{-1}. The fourth parameter can be obtained by solving P_n for $I = 0$. This is the dark respiration (R_d) which can be measured in the absence of light. P_n can also be explicitly written in function of R_d, as shown in eq. 5. where P_g stands for the gross photosynthetic rate (µmol CO_2 m^{-2} s^{-1}).

$$P_n = P_g \cdot \alpha_c \cdot \frac{I}{P_g + \alpha_c \cdot I} - R_d \qquad \text{eq. 5}$$

The fifth and final parameter is I_s, which is the light intensity which corresponds with P_n almost reaching $P_{n,max}$.

2.3 A-Ci curve

A-Ci curves indicate the net assimilation rate, P_n or A, in function of the substomatal CO_2 concentration, C_i (Manter and Kerrigan, 2004). First photosynthetic measurements have been performed on the lettuce varieties to measure P_n at different internal CO_2 concentrations (C_i). A-Ci measurements started at 400 ppm external CO_2 pressure after which the CO_2 pressure decreased to 50 ppm. The external CO_2 pressure resumed again at 400 ppm after which it was increased to 1500 ppm. The C_i pressure was slightly lower than the external pressure since this was the CO_2 pressure within the substomatal cavities.

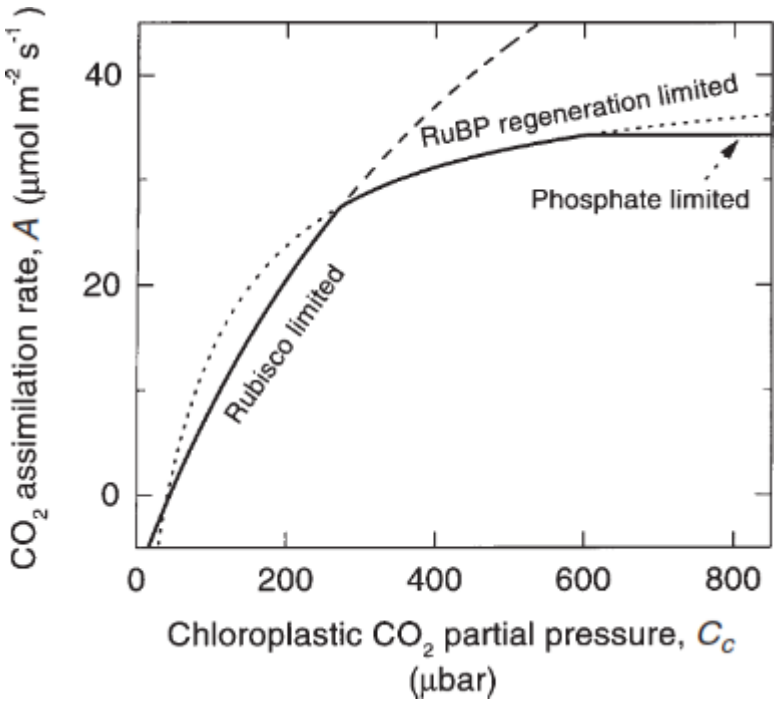

Figure 17*. The CO_2 assimilation rate to the internal CO_2 concentration as an example of an A-Ci curve represented with their subsequent limitations (von Caemmerer, 2000).*

Through use of the Farquhar-von Caemmerer-Berry model of photosynthesis in PhytoSim, the A-C_i curves were fit to the data measured with the LI-6400XT. This model is plant non-specific and was developed for C_3 plants that have similar biochemical characteristics. As such, it can be applied to lettuce. The script for the model can be found in the appendix. The model includes six parameters: $V_{c,\max}$, J, R_d, Γ_*, K_c and K_o. The following parameters can be calibrated:

- $V_{c,\max}$, the maximum carboxylation rate (µmol m^{-2} s^{-1}),
- J, the rate of electrons needed for the whole electron transport used for photosynthetic carbon reduction and photosynthetic oxidation cycles (µmol m^{-2} s^{-1}),
- R_d, the day respiration (µmol m^{-2} s^{-1}),
- Γ_* the CO_2 compensation point at 25°C (µbar). This was the CO_2 partial pressure at which the net production of the plant becomes zero. It occurs when the stomata were closed (von Caemmerer, 2000).

Other values that were plugged in as fixed or set, were:

- K_c Michaelis-Menten constant of Rubisco for CO_2 (µbar),
- K_o Michaelis-Menten constant of Rubisco for O_2 (mbar) (von Caemmerer, 2000; Manter and Kerrigan, 2004).

The model calculates the net assimilation rate A as a minimum of three functions describing A under different limiting circumstances (Figure 17, eq. 6).

$$A = \min\{A_c, A_j, A_p\} \qquad \text{eq. 6}$$

with:

Figure 18. Clipping a leaf inside the leaf chamber for photosynthesis measurements using the Li-6400XT (photographed by Huysentruyt, Jaron, 2017).

$$A_c = \frac{V_{c,max}(C_{chl} - \Gamma_*)}{C_{chl} + K_c\left(1 + \frac{O}{K_o}\right)} - R_d \quad \text{eq. 7}$$

$$A_j = \frac{J\,(C_i - \Gamma_*)}{4C_{chl} + 8\Gamma_*} - R_d \quad \text{eq. 8}$$

$$A_p = \frac{3T_p\,(C_i - \Gamma_*)}{C_{chl} - (1 + 1.5\,\alpha_{gl})\Gamma_*} - R_d \quad \text{eq. 9}$$

Here, A_c represents the RuBP-saturated rate of CO_2 assimilation (µmol m^{-2} s^{-1}) (eq. 7), A_j the RuBP-limited CO_2 assimilation rate (µmol m^{-2} s^{-1}) (eq. 8), A_p the export-limited CO_2 assimilation rate (µmol m^{-2} s^{-1}) (eq.9), C_{chl} the chloroplastic CO_2 partial pressure (mbar), O the O_2 partial pressure (mbar), and α_{gl} the fraction of glycolate carbon not returned to the chloroplast (von Caemmerer, 2000).

The limitations these formulas represents are limitations through RuBP (ribulose-1,5-bisphosphate) saturation (A_c), limitations in RuBP-regeneration (limitated by electron transport) (A_j) and through limitations in the supply of triose phosphates needed for photophosforylation (A_p) which occurr at high CO_2 partial pressure (von Caemmerer, 2000). Both RuBP and triose phosphates were essential steps in the production of glucose in the light independent reactions. In each of these three formulas, the carboxylation rate of rubisco is adjusted for the loss through respiration and oxygenation.

Although the RuBP limited CO_2 assimilation A_p can explain the CO_2 assimilation rate at the higher end of the C_i axis (Figure 17), it wasn't included in the model since there are only a small number of studies available in which triose phosphate-limited data are presented (von Caemmerer, 2000). This could have had implications for the results since measurements were also conducted at high CO_2 levels, up to 1500ppm for the A-C_i measurements. Here, this effect could be significant.

2.4 Datasets

Three datasets were made (Table 2). These datasets will be referred to as dataset 1, dataset 2 and dataset 3.

Table 2*. Summary of the different datasets. LRC stands for making a light response curve, A-CI stands for making an A-Ci curve. * plant and harvest date for Xandra, Saturdaï and Mondaï **plant and harvest date for Fairly, Lucrecia and Presteria.*

Dataset	Experiments	Varieties	Frequency	Plant date	Harvest date
1	LRC, ACI, weighing	Fairly, Lucrecia, Presteria, Xandra, Saturdaï, Mondaï	Single measurement	15/10/2016* 13/10/2016**	18/11/2016* 28/11/2016**
2	LRC, ACI, weighing	Mondaï, Xandra, Saturdaï	Weekly (5 weeks)	15/02/2017	27/03/2017
3	weighing	Fairly, Lucrecia, Presteria, Xandra, Saturdaï, Mondaï	at plant and harvest date	15/02/2017*	27/03/2017* 31/03/2017**

For the varieties Mondaï, Saturdaï, Xandra, Lucrecia, Presteria and Fairly, single day measurements were performed on almost adult plants in dataset 1. LRCs and A-Ci curves were constructed with 5 repetitions each. In dataset 2, Mondaï, Xandra and Saturdaï were measured weekly with 5 repetitions per cultivar for the LRCs and 1 repetition for the A-Ci curve. Dataset 3 was a collection of the harvest weights performed by the Research Station for Vegetable Production, Sint-Katelijne Waver. The dataset contains the measured weight of 63 plants per variety (in total 189 green and 189 red plants).

3 Model 1: Predictive models using only plant specific parameters

3.1 Introduction

During chapters 3, 4 and 5, three plant growth models will be discussed. The first one is the most simple one using only plant specific parameters such as $P_{n,\max}$. Contrary to the model of chapter 4, this model does not use changing climatic factors, or contrary to the model of chapter 5, this model does not have plant specific parameters that vary through time. The simplicity of this model is its main advantage. Measurements needed for the input can occur at a single moment during the development of the lettuce plant and do not need to be spread over the course of its growth.

In the following chapters, the word "model" will be used to only refer to the specific model discussed in that particular chapter.

3.2 The model

Plants grow under sunlight according to their carbon balance. On one side they accumulate carbon as biomass through their photosynthetic production P_g. On the other hand they respire their produced carbohydrates continuously to maintain their metabolic activity. This rate of respiration is expressed as R_d. The difference between the P_g and R_d is the carbon accumulation. This difference is called the net photosynthetic production P_n. The net photosynthetic production can be calculated using eq. 5.

To be able to evaluate the added value of models that also include dynamic light intensities, temperatures and CO_2 concentrations, this model will first be used to predict the dry weight of a lettuce plant with a fixed light intensity and without taking into account changing levels of CO_2 concentrations or temperature. P_n can also be expressed in gram by using the conversion factor (C_α) of 0.03 g glucose (µmol CO_2)$^{-1}$. C_α was derived directly from the formula of photosynthesis: $6CO_2 + 6H_2O \xrightarrow{hv} C_6H_{12}O_6 + 6O_2$. When converted using their respective molecular masses to weights in grams, 1 mole of CO2 sequestrated results in 30 g of glucose. The contribution of R_d can be calculated by solving eq. 5 for $I = 0$. Also here, this value can be expressed per gram after converting it through the conversion factor of 0.03 g glucose (µmol CO_2)$^{-1}$.

During the daytime both P_g and R_d were taken into account while during the night only R_d had an effect (eq. 11, eq. 12). This will result in the day-night pattern that could be seen in the dry weight of the plant. Larger plants tend to have a larger photosynthetic production by having more leaf area or photosynthetically active surface, and tended to have a larger respiration. That is why P_g and R_d are proportionate with the dry weight X_d. Van Henten proposed a proportionality constant of $5 \cdot 10^{-6}$ s^{-1} for a similar use (Van Henten, 1994). This value was adjusted after calibration and will be presented later on during the results sections. This results in the following expressions:

$$(day) \qquad \frac{d(X_d)}{dt} = P_g \cdot C_{proport} \cdot X_d + R_d \cdot C_{proport} \cdot X_d \qquad \text{eq. 11}$$

$$(night) \qquad \frac{d(X_d)}{dt} = R_d \cdot C_{proport} \cdot X_d \qquad \text{eq. 12}$$

Here $C_{proport}$ stands for a proportionality factor which accounts for the positive feedback between growth and photosynthesis. More photosynthesis results in more biomass, which in its turn results in more

photosynthetically active leaf area. The biomass production of lettuce can be expressed in different ways. Besides expressing it in dry mass X_d (g m^{-2}), it can also be expressed in dry weight per plant or fresh weight per plant or per square meter. According to Van Henten (1994), lettuce plants are often cultivated with 18 plants per square meter and since lettuce is 95.56 % made out of water, a conversion factor of 22.5 fresh mass to dry mass can be used. PSKW often uses seedlings with a mass between about 1 and 5 g. Assuming for the model that seedlings had a weight of 4.50 g, this resulted in 3.60 g m^{-2} dry mass of seedlings. This was chosen as the initial value for the derivatives for X_d.

3.3 Climatic constants

This model doesn't require an input for the climatic conditions: temperature, CO_2 concentration and incident radiation. The climatic factors were included as constants to be able to calculate the net photosynthetic production P_{net}. The value for the total average PAR radiation that reached the canopy was set at 374.14 µmol m^{-2} s^{-1}. This value corresponded to 240 W m^{-2}, used by Van Henten (1994) which was an average that also takes the night into account. 240 W m^{-2} as average incident radiation was confirmed by similar data at PSKW. For the conversion to µmol m^{-2} s^{-1} two conversion factors for diffuse and for direct sunlight were used (Table 3).

***Table 3**: Conversion factors from W m^{-2} to µmol m^{-2} s^{-1} for both diffuse sunlight and direct sunlight (Blindeman et al., 2015)*

Conversion factors from W m^{-2} to µmol m^{-2} s^{-1}	
for diffuse sunlight	**for direct sunlight**
4.57	4.24

Since on average only 35.30 % of days in Belgium have clear weather, a weighted average of 4.454 was used. Considering only 70 % of light transmits through the greenhouse glass, and only 50 % of incident light was PAR, only 84 W m^{-2} of the 240 W m^{-2} remained. This corresponded to the 374.14 µmol m^{-2} s^{-1} which was used in the model (eq. 13).

$$PAR\left(\frac{\mu mol}{m^2 \cdot s}\right) = radiation_{average} \cdot C_{unitconversion} \cdot C_{transmission} \cdot C_{fractionPAR} = 240\frac{W}{m^2} \cdot 4.454\frac{\mu mol}{W \cdot s}0.7 \cdot 0.5 = 374.14\ \frac{\mu mol}{m^2 \cdot s} \quad \text{eq. 13}$$

3.4 Inputs

The inputs for this model (Table 4) were the parameters derived from the LRCs that could easily be constructed in PhytoSim with the data of the LI-6400XT. These were $P_{n,\max}$ µmol m^{-2} s^{-1}, α_c (µmol CO_2 (µmol photons)$^{-1}$) and I_c (µmol m^{-2} s^{-1}).

***Table 4**: The plant specific inputs (and only inputs) for model 1.*

Parameter	Unit	Xandra	Saturdaï	Mondaï	Average
$P_{n,max}$	µmol m^{-2} s^{-1}	13.283	15.6678	16.8025	15.2511
α_c	-	0,070519	0,084692	0,101341	0,085518
I_c	µmol m^{-2} s^{-1}	13,4352	13,0604	14,0405	13,51203

3.5 Mass data used for calibration

Calibration of the results could occur with two different methods. The first method of calibration is a calibration which only uses the starting mass of the seedling and the harvest mass while the second method of calibrating to the weight also considered the weekly weights between plant and harvest. Not needing the intermediary weights of the lettuce plants would significantly simplify the development of new models. The calibration method which includes the weekly weights included the last data pair of age and mass three times, since the end weight was more important than the intermediary weights. Both calibration methods were used to compare their results.

4 Model 2: Predictive models using both plant specific and climate factors

4.1 Introduction

One of the major aims of horticulture crop production shows higher economic results through better crop production under controlled climatic conditions. For example, having lettuce grown at 800ppm CO_2 instead of 350ppm increases the average weight increase with 20 % (Van Henten, 1994). That is why Van Henten worked out a model that takes into account the CO_2 concentration (X_c), the solar radiation at canopy level (V_i) and the temperature of the grow environment (X_T). With this model, the trade-off between cost of operation to sustain climatic conditions and economic return can be evaluated.

The Van Henten Model acted as the basis for the mechanistic approach that includes the climatic conditions. The plant specific parameters were incorporated using data output of the portable photosynthesis system, LI-6400XT. The data was processed using PhytoSim in order to extract certain parameters, being the ($P_{n,max}$), the stomatal H_2O conductivity ($Cond$), the boundary layer H_2O conductivity ($BLCond$) and the CO_2 compensation point at 25°C ($C_{comp,25}$). With this model a methodology will be proposed for easy and reliable screening of plants.

What distinguished this model from the previous one is the second type of inputs. Besides having plant specific inputs, model 2 also works with climatic inputs being temperature X_T (°C), radiation V_i (W m^{-2}) and CO_2 concentration X_c (kg m^{-3}). The model also includes two types of parameters with each set having its own calibration. The distinction is a consequence of the model structure which will be explained during the next section.

This method can also be applied for other varieties but this would first require tracking the weight of plants with known similar characteristics such as morphology (leaf configuration) or metabolism. After tracking the weight, the set 2 parameters could yet again be calibrated to the biomasses. With the model and obtained set 2 parameters, new similar plants in this group can be screened easily.

4.2 The model

The following model is the Van Henten model and makes up the core of this model. It predicts the dynamic behaviour of the biomass taking biochemical processes into account such as photosynthesis, dark respiration and photorespiration. The parameters whose values were not mentioned are parameters that were determined by photosynthesis measurements and are discussed under the results section.

$$\frac{d(X_d)}{dt} = C_\beta \cdot \left(C_\alpha \cdot \Phi_{phot} - \Phi_{resp}\right) \qquad \text{eq. 14}$$

The increase in dry weight production of the lettuce plant is based on the difference between the photosynthetic production Φ_{phot} and the respiration Φ_{resp} as presented by eq. 14. In this expression, C_α was the conversion factor for CO_2 into glucose. A value of 0.68 was chosen. This value was used by Van Henten and merely was the ratio of the molecular weight of glucose to six times the molecular mass of CO_2 which is needed to make one glucose molecule (Van Henten, 1994). C_β was the conversion factor for carbohydrates to structural dry weight of the plant. It indicates the synthesis and respiratory losses of non-structural material during growth. Non-structural dry weight consists for instance of glucose, sucrose and starch while structural dry weight consists of structural components such as cell walls and cytoplasm. Specific to lettuce, Sweeney *et al.* (1981) found a value of 0.80 for C_β while Van Keulen *et al.* (1982) estimated the

value to be 0.72. The calibration range for this parameter was wide enough to include both values (Van Henten, 1994).

The response of canopy photosynthesis Φ_{phot} to the PAR and the CO_2 concentration id described by eq. 15, with C_{lard} (m^2 kg^{-1}) the proportionality constant for leaf area derived from the dry matter. According to measurements of Lorenz and Wiebe (1980) C_{lard} was estimated to be $75 \cdot 10^{-3}$ m^2 kg^{-1}. A higher dry mass X_d would result in a higher leaf area, which resulted in larger plant photosynthesis production. C_k is the light extinction coefficient. It considers the scattering of the light depending on the leaf position. For planophile plants C_k is 0.9, while for erectofile plants, 0.3 is more suitable. Lettuce is more planophile than erectofile so a value of 0.9 was chosen. The calibration boundaries were chosen wide enough to include both values. (Goudriaan and Monteitht, 1990; Van Henten, 1994). C_τ represents the fraction of underground dry mass to the total dry mass. A value of 0.15 was reported specifically for lettuce grown in soil by Lorenz & Wiebe (1980).

$$\Phi_{phot} = \Phi_{phot,max} \cdot \left(1 - e^{(-C_k \cdot C_{lard} \cdot (1-C_\tau) \cdot X_d)}\right) \quad \text{eq. 15}$$

With:

$$\Phi_{phot,max} = \frac{\varepsilon \cdot (C_{PAR} \cdot C_{radrf} \cdot V_i + V_{LED}) \cdot \sigma_{CO2} \cdot (X_c - \Gamma)}{\varepsilon \cdot (C_{PAR} \cdot C_{radrf} \cdot V_i + V_{LED}) + \sigma_{CO2} \cdot (X_c - \Gamma)} \quad \text{eq. 16}$$

$\Phi_{phot,max}$ (g m^{-2} s^{-1}) is the maximum response of canopy photosynthesis under certain conditions of incident radiation V_i (W m^{-2}), temperature T (°C) and CO_2 concentration X_c (kg m^{-3}) (eq. 16). Additional radiation through LEDs is represented by V_{LED} in (W m^{-2}) and will be explained further on. σ_{CO2} (m s^{-1}) represents the canopy conductance for CO_2 diffusion from the ambient air to the chloroplast. It's defined by three conductance's as presented in eq. 17. Two are physical in nature, the stomatal conductance C_{stm} (m s^{-1}) and the boundary layer conductance C_{bnd} (m s^{-1}), while the third one is chemical of nature, the carboxylation conductance σ_{car} (m s^{-1}). As shown in eq.19, σ_{car} depends on three biochemical parameters of which their values, according to Goudriaan et al. (1985) (Van Henten, 1994). The lowest conductance will predominantly determine the diffusion speed of CO_2. $C_{rad,rf}$ is the constant for the transmission through the glass roof, which has improved since Van Henten proposed this model from 0.5 according to Van Henten (1994) to 0.7 recent years (Blindeman et al., 2015). C_{PAR} is the fraction of PAR to the total incident radiation.

$$\sigma_{CO2} = \left(C_{bnd}^{-1} + C_{stm}^{-1} + \sigma_{car}^{-1}\right)^{-1} \quad \text{eq. 17}$$

With

$$\sigma_{car} = C_{car1} \cdot X_t^2 + C_{car2} \cdot X_t + C_{car3} \quad \text{eq. 18}$$

The maintenance respiration of the lettuce crop is expressed as eq. 19, with C_{respr} and C_{resps} the respiration parameters for the underground and aboveground parts of the plant at 25 °C. This is expressed as the mass of glucose consumed per unit mass of dry matter. According to Van Keulen (1982) these are 0.03 and 0.01 per day. $C_{Q10resp}$ represents the increase in respiration for an increase in temperature by 10 °C. A value of 2 was used by Van Henten (1994), while Von Caemmerer (2000) proposed a value of 1.37. Both values were taken into consideration for calibration. A feedback from the dry weight can be found here. A larger biomass will result in a higher respiration.

$$\Phi_{resp} = \left(C_{resps} \cdot (1 - C_\tau) + C_{respr} \cdot C_\tau\right) \cdot X_d \cdot C_{Q10resp}^{\frac{X_t - 25}{10}} \quad \text{eq. 19}$$

The Model of Van Henten also used the CO_2 concentration, and light intensity for its calculations besides temperature. The temperature has an influence on the CO_2 compensation point Γ (ppm) which is an

indicator for photorespiration at high levels of PAR. Γ is affected by the temperature according to eq. 20. X_c was also used in this model and has an influence on the light use efficiency ε (g J^{-1}). While photorespiration at high PAR levels only has an observable effect at the CO_2 compensation point, it has a pronounced effect on the light use efficiency ε at lower light levels, which is approximated in eq. 21. In this equation C_ε (g J^{-1}) is the parameter for light use efficiency at high CO2 concentration and no photorespiration (Van Henten, 1994). According to Goudriaan *et al.* (1985) C_ε and $C_{Q10\Gamma}$ have values of $1.70 \cdot 10^{-6}$ and 2 g J^{-1}.

$$\Gamma = C_\Gamma \cdot C_{Q10\tau}^{\frac{X_t - 20}{10}} \quad \text{eq. 20}$$

$$\varepsilon = C_\varepsilon \cdot \frac{X_c - \Gamma}{X_c + 2 * \Gamma} \quad \text{eq. 21}$$

To avoid large fluctuations in the growth rate of the plant, a capping of the CO_2 conductivity σ_{CO2} (eq. 22) was needed as X_d could be heavily influenced by an extreme σ_{CO2}.

$$\sigma_{CO2} = \left(\frac{1}{C_{bnd}} + \frac{1}{C_{stm}} + \frac{1}{\sigma_{car}}\right)^{-1} \quad \text{eq. 22}$$

Extremely high σ_{CO2} could occur when σ_{car} approaches its asymptotic value. This value, can be derived from eq. 23.

$$\sigma_{car_{asympt}} = \left(-\frac{1}{C_{bnd}} - \frac{1}{C_{stm}}\right)^{-1} \quad \text{eq. 23}$$

For this model the value of $\sigma_{car_{asympt}}$ amounted to -0.001338 m s^{-1}. This negative σ_{car} was a result of high temperatures (exceeding 25 °C). These extreme high CO_2 conductivities were a mathematical artefact of the approximation of the real CO_2 conductivity, and a capping was needed on its values. A first boundary was implemented as a lower limit at 0 m s^{-1}, since conductivity cannot be negative. A second boundary was the upper limit. Most calculated CO_2 conductivities derived from the used climatic data were clearly limited to a maximum of 0.0004 m s^{-1}, which was only exceeded three times. This continuously recurring value of 0.0004 m s^{-1} was chosen as the upper limit.

4.3 Inputs of the model

The model has two types of inputs: climatological inputs and plant specific inputs. The first type are climate data inputs, which are tables that contained the temperature, CO_2 concentration and incident radiation per hour for the entire grow period. These were measured continuously by PSKW (Figure 21).

Figure 19. The lettuce plants in the morning when the LED lights were still on (photographed by the author, 2017).

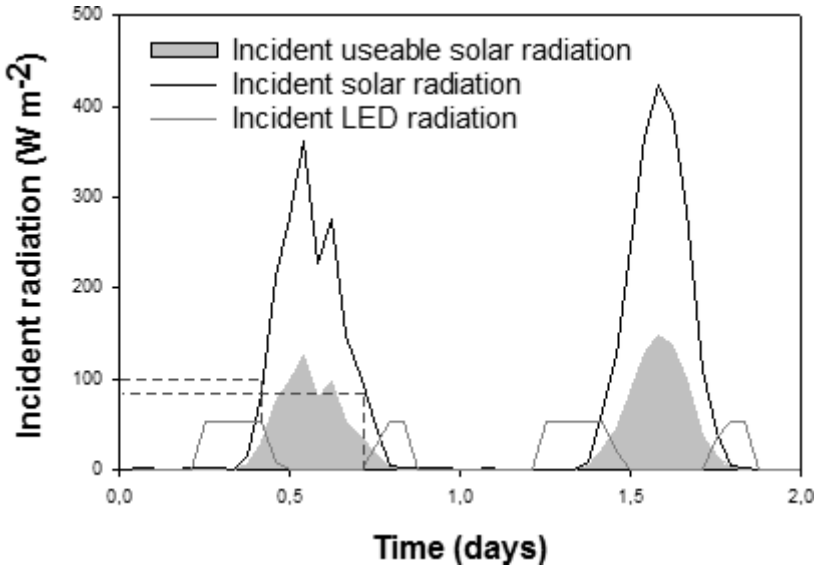

Figure 20. *A close up of the radiation input data. The red lines indicate the 100 and 80 W m^{-1} at which the lamps switch off and switch back on again. The incident useable solar radiation is depicted to be able to compare with the LED radiation.*

To be able to take additional lighting through LEDs into account, a second radiation can be used through data variable V_{LED}. This input is similar to the regular incident radiation and contains the incident radiation in W m^{-2} per hour. The LED intensity and the PAR fraction reaching the canopy of the incident solar radiation was summated for the calculation of $\Phi_{phot,max}$. The LEDs can only be fully on or fully off. The lamps switch on before sunrise and switch off again when the sunlight reaches 100 W m^{-2}. The lamps switch on again when the solar radiation reaches a intensity as low as 80 W m^{-2} during the evening, as indicated in Figure 20 with dashed lines. The amount of LED light energy reaching lettuce canopy had an average value of 177 µmol m^{-2} s^{-1}, as measured at PSKW during the LightMan project (Proefstation voor de Groeneteelt, 2016). This resulted in a pink appearance of the lettuce plants as shown in Figure 19. To compare this with the incident solar radiation, it still requires a conversion of the photosynthetic photon flux density in µmol m^{-2} s^{-1} to W m^{-2}, which was not the same for LEDs as it was for solar radiation or other light sources. According to grow lamp producer information the conversion factor for LED light being 95 % red and 5% blue is 2.2 µmol m^{-2} s^{-1} (Philips Company, 2017).

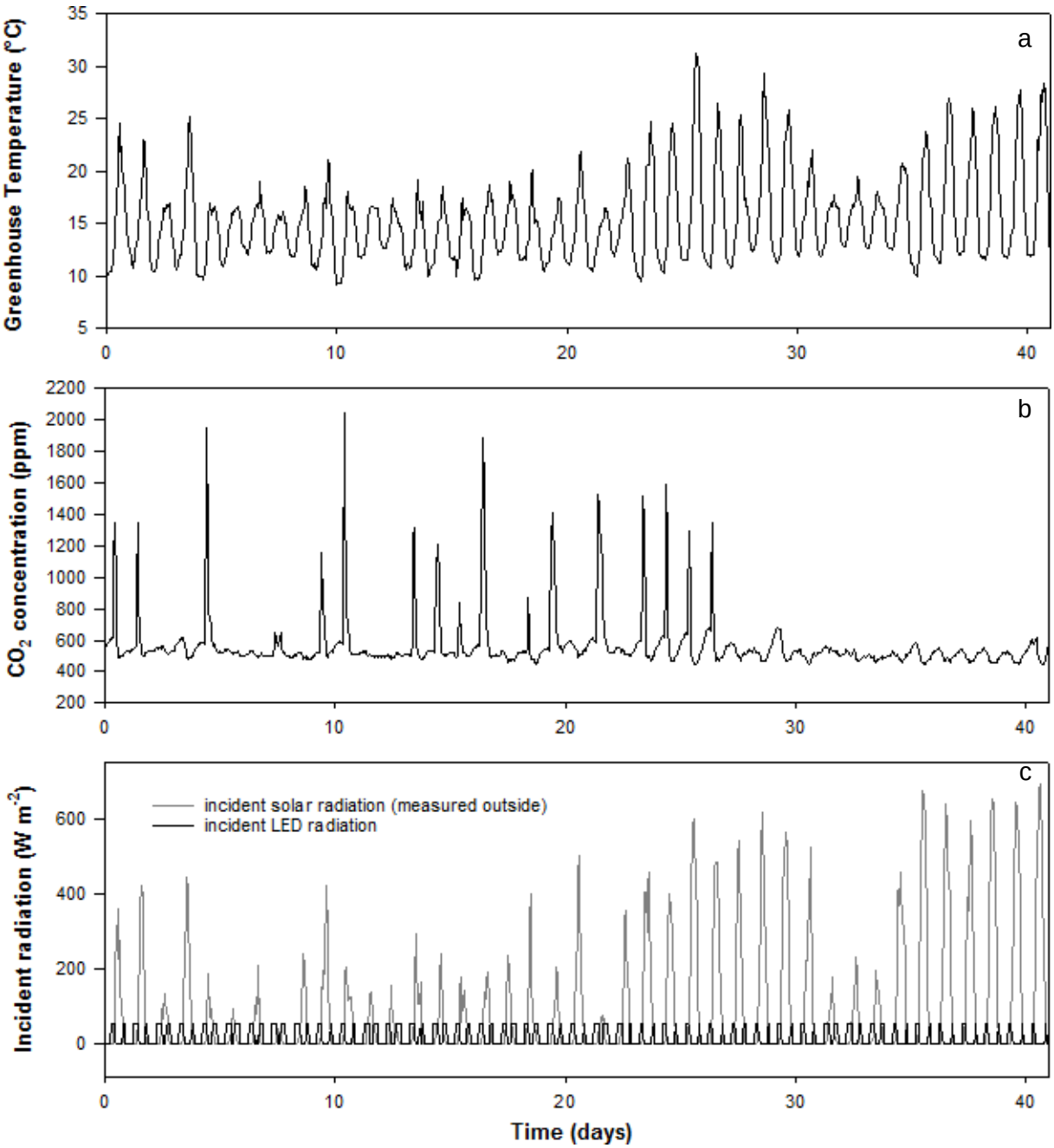

Figure 21. *The climatic inputs of model 2. (a) The greenhouse temperature (b) the CO_2 concentration and (c) the incident radiation as measured outside of the greenhouse together with the incident LED radiation which was 100% PAR.*

The second inputs are the parameters that were measured during screenings with the LI-640XT. To be able to study the outcome of a model based on one-time measurements. Measurements were used from the final week before harvest. During the weeks of measurements, LRCs were made for both red and green lettuce varieties. The values used were part of dataset 2. The used parameters were those presented in Table 5.

Table 5. *The plant specific parameters which could be calibrated using the outputs of the LI-6400XT.*

Model inputs	Units	Name	Measurable link to the plant	Units	Name
C_{stm}	m s^{-1}	Stomatal CO_2 conductance	$Cond$	mol m^{-2} s^{-1}	Stomatal H_2O conductance
C_{bnd}	m s^{-1}	Boundary layer CO_2 conductance	$BLCond$	mol m^{-2} s^{-1}	Boundary layer H_2O conductance
C_Γ	g m^{-3}	CO_2 compensation point at 20°C	$C_{comp,25}$	µbar	CO_2 compensation point at 25°C
$\Phi_{phot,max}$	g m^{-2} s^{-1}	response of canopy photosynthesis	$P_{n,max}$	mol m^{-2} s^{-1}	Maximum net photosynthetic production

The LI-6400 XT could not directly measure C_{stm}, C_{bnd}, C_Γ and $\Phi_{phot,max}$. The first three could be determined by using related measured physiological parameters. On the other hand, for the fourth parameter $\Phi_{phot,max}$, $P_{n,\max}$ is not inserted directly but is used to calibrate all underlying parameters.

In the case of the CO_2 conductances, for the first two plant specific parameters, the known relations between water diffusion and CO_2 diffusion were applied since the LI-6400 XT only measures the water conductance. It was proven that in the stomata, the ratio of the diffusion rates for water and CO_2 equals 1.6 (Bakker, 1995). In the boundary layer, this value decreases to 1.37. With this relation the conductances for CO_2 in the stomata and in the boundary layer could be derived from the conductances of water (eq. 24, 25) with g_{st,H_2O} and g_{st,H_2O} being the stomatal conductance to CO_2 and water vapour in mol CO_2 m^{-2} s^{-1} and mol H_2O m^{-2} s^{-1} and g_{bnd,CO_2} being the boundary layer conductance to water vapour in mol H_2O m^{-2} s^{-1}.

$$C_{stm}\left(\frac{m}{s}\right) = \frac{g_{st,CO_2}\left(\frac{mol}{m^2 \cdot s}\right)}{40.876\left(\frac{mol}{m^3}\right)} = \frac{g_{st,H_2O}\left(\frac{mol}{m^2 \cdot s}\right)}{1.6 \cdot 40.876\left(\frac{mol}{m^3}\right)} = \frac{Cond\left(\frac{mol}{m^2 \cdot s}\right)}{1.6 \cdot 40.876\left(\frac{mol}{m^3}\right)} \quad \text{eq. 24}$$

$$C_{bnd}\left(\frac{m}{s}\right) = \frac{g_{bnd,CO_2}\left(\frac{mol}{m^2 \cdot s}\right)}{40.876\left(\frac{mol}{m^3}\right)} = \frac{g_{st,H_2O}\left(\frac{mol}{m^2 \cdot s}\right)}{1.37 \cdot 40.876\left(\frac{mol}{m^3}\right)} = \frac{BLCond\left(\frac{mol}{m^2 \cdot s}\right)}{1.37 \cdot 40.876\left(\frac{mol}{m^3}\right)} \quad \text{eq. 25}$$

The third plant specific parameter, $C_{comp,25}$ wasn't measured by the LI-6400XT. It was computed through the use of the model of Von Caemmerer – Farquhar by constructing A-C_i curves. But even then the compensation point was only valid for a temperature of 25°C while the Van Henten model needs this value at 20°C. This could easily be converted by correcting for its temperature by eq. 26. After this, only a conversion of units was needed to be able to plug in the suited CO_2 compensation point, such as eq. 27.

$$C_{comp,20}\ (\mu bar) = C_{comp25}\ (\mu bar) \cdot Q_{C,comp}^{\frac{20°C-25°C}{10°C}} \quad \text{eq. 26}$$

$$C_\Gamma\left(\frac{g}{m^3}\right) = C_{comp,20}(\mu bar) \cdot 10^{-6}\left(\frac{bar}{\mu bar}\right) \cdot 0.9862\left(\frac{atm}{bar}\right) \cdot \left(\frac{1}{atm}\right) \cdot \frac{1.94\left(\frac{g}{m^2}\right)}{ppmv} \quad \text{eq. 27}$$

The fourth plant specific parameter, the response of canopy photosynthesis $\Phi_{phot,max}$ was also not directly measurable. The closest measurable parameter was the maximum $P_{n,\max}$.

4.5 Calibration procedure

The model included two types of parameters with each set having its own calibration, as shown in Figure 22. The first set of parameters were all the parameters that together determine $\Phi_{phot,max}$ and was evidently referred to as set 1 parameters. This set of parameters was determined by calibrating the $\Phi_{phot,max}$ in the model to the $P_{n,max}$ originating from the LI-6400XT and will be different for every future plant measured. But contrary to $\Phi_{phot,max}$, $P_{n,max}$ was fixed. $P_{n,max}$ did not vary in function of the incident radiation. However, plotting $\Phi_{phot,max}$ in function of the incident radiation or X_c indicated that $\Phi_{phot,max}$ stagnated at high V_i and X_c, about 1000 W m^{-2} and 1200 ppm. This implied that $P_{n,max}$ should equal $\Phi_{phot,max}$ at light saturating and CO_2 saturating conditions. The calibration of the $\Phi_{phot,max}$ comprising parameters to match $\Phi_{phot,max}$ to $P_{n,max}$, was the first step in the parameter calibration. Further on, this set of parameters is referred to as the set 1 parameters and are: C_{lard}, C_{car1}, C_{car2}, C_{car3}, $C_{Q10\Gamma}$ and C_{ε}.

The second set includes all other model parameters and were calibrated to a known average harvest weight of an average red lettuce population with average plant specific parameters. Using a known average harvest mass for calibration was necessary because one cannot calibrate the model parameters to the individual harvest mass if this was what one intended to predict. That was why this thesis used an average population with a known average biomass within a certain plant variety population, being here red lettuce.

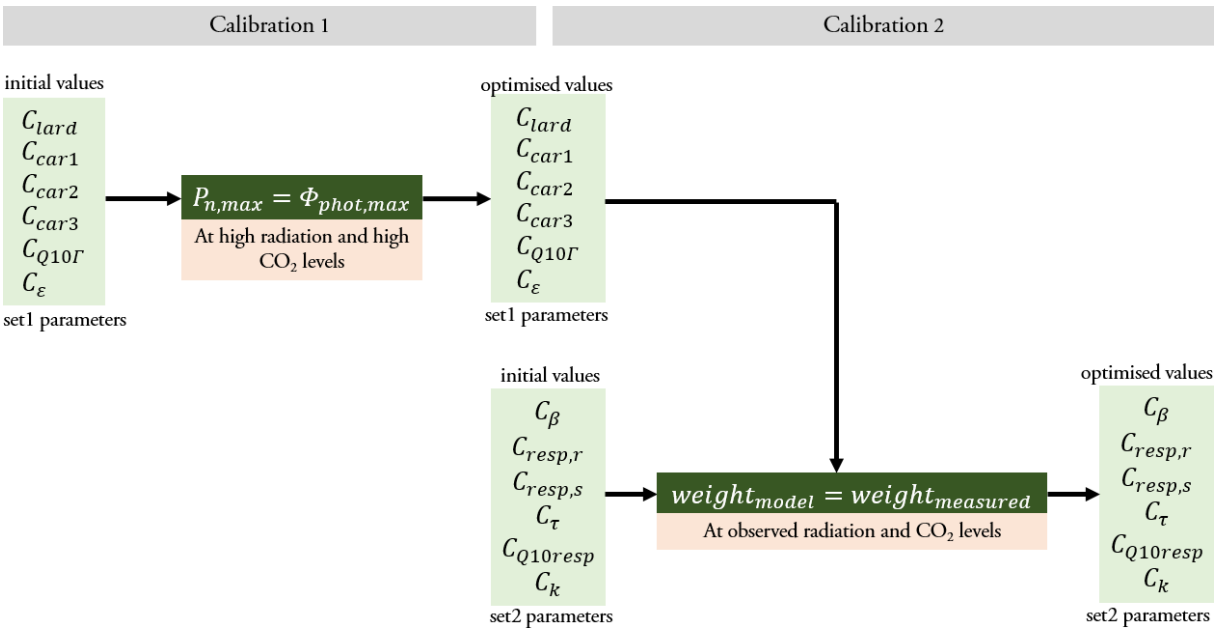

Figure 22*. An overview of the two step calibration procedure. For calibration 1, 6 parameters were optimised so the modelled $\Phi_{phot,max}$ equals the measured $P_{n,max}$. During this calibration radiation and CO_2 levels were kept high. For calibration 2, 6 other parameters were optimised so the modelled weight would equal the measured weight. For this observed radiation and CO_2 levels were used for the calculations.*

5 Model 3: Predictive models using both climatic and dynamic plant specific-parameters

5.1 Introduction

To evaluate if it was useful to build the model using changing plant parameters through time, a static model (chapter 3 and 4) will be compared to a dynamic model. The dynamic model will vary the plant specific inputs as measured through time being: C_{stm}, C_{bnd}, $\Phi_{phot,max}$, C_{Γ}.

5.2 Similarities and differences between the model build-up of model 2 and model 3

The model largely used the structure of the model of chapter 4 with the only difference being the four plant specific parameters changing through time.

Again there were two types of inputs: the plant specific parameters and the climatic inputs. For the plant specific inputs, LRC and A-Ci measurements were conducted on Xandra, Saturdaï and Mondaï 5 times on a weekly basis (Figure 23). The missing values were obtained through interpolation and extrapolation.

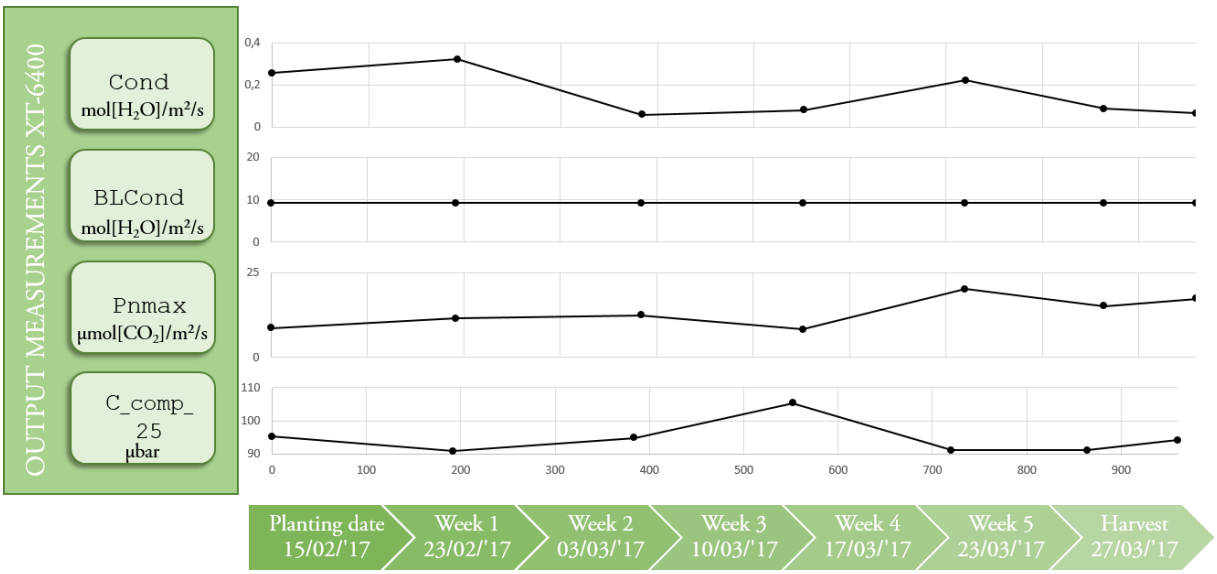

***Figure 23**. The plant specific inputs that were only being used for model 3 are: the stomatal H2O conductivity, the boundary layer H_2O conductivity, the maximum photosynthetic production and the CO_2 compensation point at 25°C. the first two were calculated directly by the LI-6400XT while the latter two were calculated through LRCs and A-Ci curves.*

The climatic inputs, being temperature, X_T, CO_2 concentration, X_c and incident radiation V_i were the same as used in the plant specific parameter-static model of previous chapter. These were registered by the climate computer.

Just like the general build-up of the model, the same calibration of the parameters was used. The calibration consisted of two parts. First calibrating the set 1 parameters being: C_{lard}, C_{car1}, C_{car2}, C_{car3}, $C_{Q10\Gamma}$ and C_{ε} which were optimised through comparing $P_{n,max}$ to $\Phi_{phot,max}$ at maximum X_c and V_i. The second calibration aimed at optimising all other parameters by comparing the predicted weight to the measured weight. These parameters were the set 2 parameters being: C_{β}, $C_{resp,r}$, $C_{resp,s}$, C_{τ}, $C_{Q10resp}$ and C_k. This procedure is illustrated in Figure 22.

Calibration 1 is completely similar to the calibration 1 of model 2. The only differences are that (i) the calibration of $\Phi_{phot,max}$ uses the dynamic $BLCond$, $Cond$ and $C_{comp_{25}}$ and (ii) calibration 1 was performed as a moving window calibration. The result of this moving window calibration were optimised parameters which vary through time. Calibration occurs in a frame with particular window size which moves through the 960 hours of growing. One calibration was performed per frame, after which the frame moves one period of time further. For the set-up of this model, a period of 48 hours and window size of 48 hours were chosen to achieve the best results.

The results of calibration 1 are vectors with a length of 20 optimised values per parameter, one for each calibration window. These were adjusted through interpolation in excel to vectors of 960 elements long per set 1 parameter. Each element representing a value for each hour. These set 1 parameters needed to be reintroduced to the model as data variables containing the vectors.

Chapter 4
Results

1 Results translating data to plant specific parameters

1.1 Dataset 1: Single A-Ci and LRC measurements

The data of the six lettuce species: Presteria, Lucrecia, Fairly, Xandra, Saturdaï and Mondaï were submitted to the procedure of making an LRC (Figure 24) or A-Ci curve (Figure 25) as described under chapter 2 of materials and methods. The parameters $P_{\max}$, α_c and I_c, were determined using PhytoSim. For the A-Ci parameters, the model of Farquhar was applied (Table 6). The computed J and R_d were their values at the standard temperature at 25 °C.

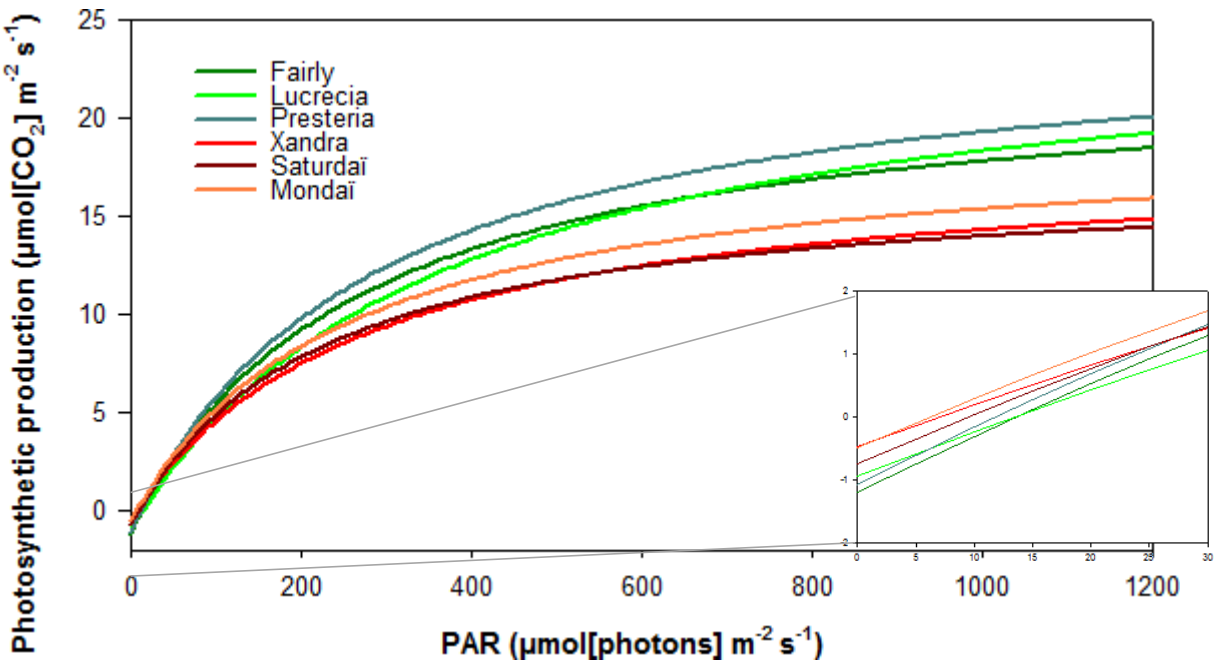

Figure 24. *The LRCs used to determine plant specific parameters P_{max} , α_c and I_c.*

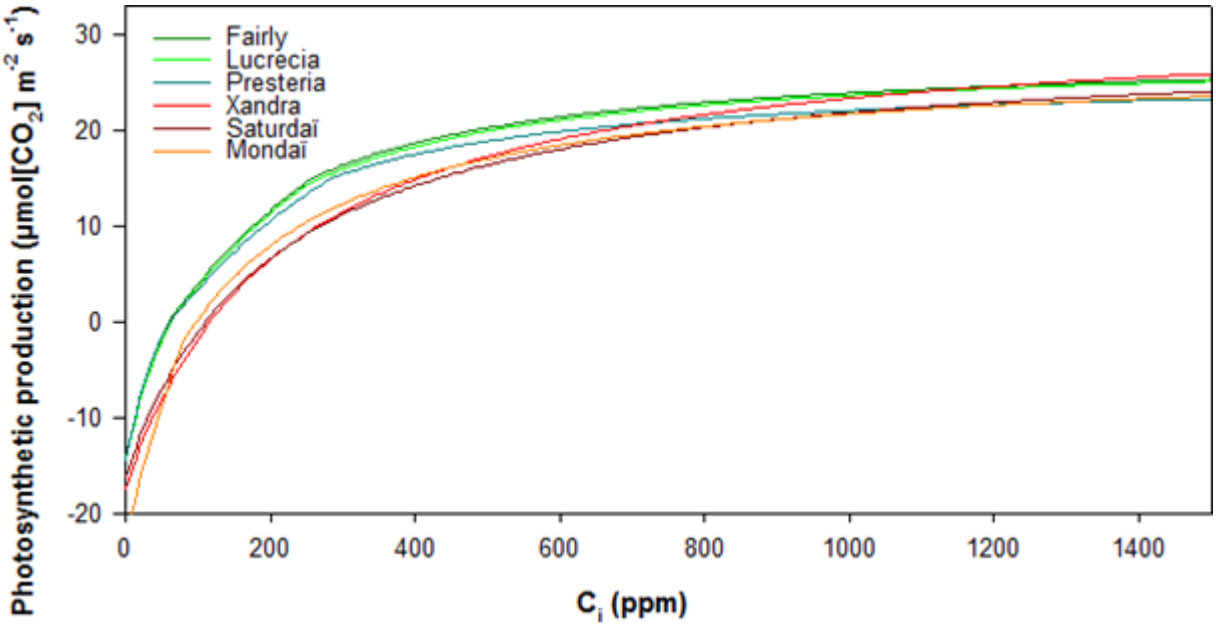

***Figure 25**. The constructed A-Ci curves to determine plant specific parameters J and R_d.*

***Table 6**. The plant specific parameters computed using the LRC and A-Ci curve which could be constructed with the data of the one day measurements with the Li-6400XT.*

	Fairly	Lucrecia	Presteria	Xandra	Saturdaï	Mondaï
From LRC						
$P_{n,max}$	22,69	25,36	24,95	18,28	17,16	19,23
α_c	0,083	0,0671	0,086	0,066	0,076	0,077
I_c	13,53	13,48	11,80	6,85	9,37	6,07
From A-Ci						
$V_{c,max}$	69,66	69,9	80,08	58,36	57,11	55,61
R_d	5,41e-05	0,49	0,056	0,85	1,85	0,73
J_{max}	151,27	153,6	154,4	218,78	190,69	172,03

1.2 Dataset 2: Weekly ACI and LRC measurements

Also for dataset 2, LRCs and A-C_i curves have been constructed which resulted in the plant specific parameters as presented in Table 7 and Table 8.

***Table 7**. The plant specific parameters of Xandra and Saturdaï computed using the LRC and A-Ci curve which could be constructed with weekly measurement data.*

	Xandra				Saturdaï			
	$\Phi_{phot,max}$ [g m^{-2} s^{-1}]	C_{stm} [m s^{-1}]	C_{bnd} [m s^{-1}]	C_{comp25} [µbar]	$\Phi_{phot,max}$ [g.m^{-2}.s^{-1}]	C_{stm} [m s^{-1}]	C_{bnd} [m s^{-1}]	C_{comp25} [µbar]
Week 1	5,07 e-4	3,79 e-3	0,165	20,70	5,24 e-4	5,80 e-3	0,165	125,99
Week 2	6,48 e-4	1,10 e-3	0,165		5,99 e-4	1,08 e-3	0,165	
Week 3	5,06 e-4	1,67 e-3	0,165	123,95	2,99 e-4	1,35 e-3	0,165	69,66
Week 4	8,74 e-4	3,45 e-3	0,165	99,91	9,29 e-4	3,77 e-3	0,165	82,48
Week 5	5,84 e-4	1,26 e-3	0,165	91,23	6,88 e-4	1,41 e-3	0,165	

***Table 8**. The plant specific parameters of Mondaï and the average red population computed using the LRC and A-Ci curve which could be constructed with weekly measurement data.*

	Mondaï				Average red population			
	$\Phi_{phot,max}$ [g m^{-2} s^{-1}]	C_{stm} [m s^{-1}]	C_{bnd} [m s^{-1}]	C_{comp25} [µbar]	$\Phi_{phot,max}$ [g m^{-2} s^{-1}]	C_{stm} [m s^{-1}]	C_{bnd} [m s^{-1}]	C_{comp25} [µbar]
Week 1	4,91 e-4	5,14 e-3	0,165	126,00	5,07 e-4	4,914 e-3	0,165	90,89
Week 2	4,04 e-4	0,58 e-3	0,165		5,50 e-4	0,924 e-3	0,165	
Week 3	2,86 e-4	0,70 e-3	0,165	122,42	3,63 e-4	1,244 e-3	0,165	105,34
Week 4	8,57 e-4	3,00 e-3	0,165	91,23	8,87 e-4	3,412 e-3	0,165	91,21
Week 5	7,38 e-4	1,37 e-3	0,165		6,70 e-4	1,350 e-3	0,165	91,23

2 Results predictive model using only plant specific parameters

2.1 Calibration and parameter values

The following parameters were calibrated within their respected ranges (Table 9). The initial values chosen were values found in literature and used by Van Henten (1994). Besides for $C_{proport}$, the ranges were set on a range of 40 % lower and higher than the initial value. Since the weights of the plants during their last weeks were more important than during their first weeks, the last point was considered as three overlapping points during calibration. None of the three optimising parameters were limited by their boundaries during calibration.

***Table 9**. The calibration boundaries within which the optimising variables of model 1 were varied.*

Parameter	Initial value	(-40%) Lower boundary	(+40%) Upper boundary	Units	Source
$C_{proport}$	5.000e-6	3e-7	7e-4	-	Van Holstein (1981)
$C_{resp,s}$	3.4722e-7	2.08e-7	4.86e-07	s^{-1}	Van Keulen *et al.* (1982)
$C_{resp,r}$	1.16e-7	6.96e-08	1.62e-07	s^{-1}	Van Keulen *et al.* (1982)

After calibrating the model to fit mass data of Xandra, Saturdaï and Mondaï in dataset 2, which was weighted every week, the following values as shown in Table 10 were obtained:

***Table 10**: Calibrated parameter values for the average red lettuce variety population of model 1.*

Parameter	Calibrated value	Unit
$C_{proport}$	3.53916e-05	m^2 g^{-1}
C_{resps}	3.73919e-07	s^{-1}
C_{respr}	1.41526e-07	s^{-1}

2.2 Modelled growth

For the individual red lettuce varieties: Xandra, Saturdaï and Mondaï, model simulations were made (Figure 28 (a)). The same was done for the average red lettuce population in Figure 28 (b), and for the average red and average green variety population by only using mass data of the plant and harvest days (Figure 28 (c)).

The average red population model has also been applied on Xandra, Saturdaï and Mondaï to evaluate its ability to predict their masses based on the plant specific parameters of these individual varieties (Figure 26 (a)).

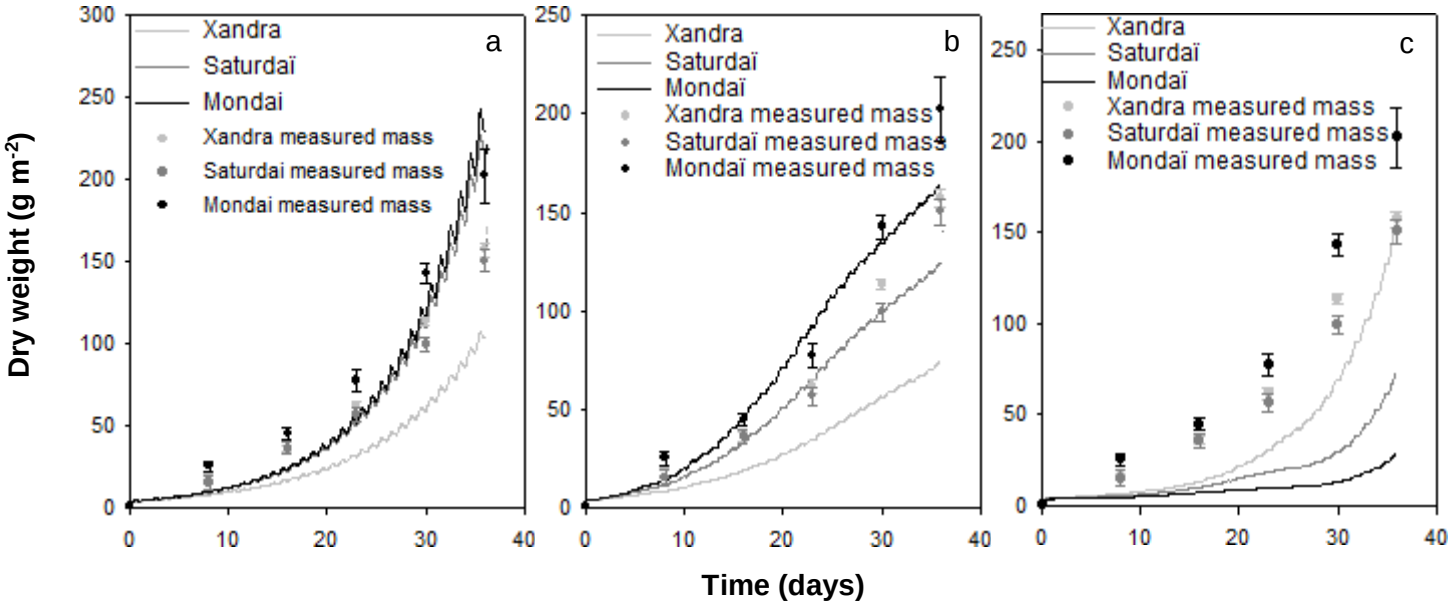

***Figure 26**: The model outputs for (a) model 1, (b) model 2 and (c) model 3 where the models were used as a general model that was trained to the average red variety lettuce population mass data and used to predict the growth of Xandra, Saturdaï and Mondaï based on their plant specific inputs.*

To illustrate the exponential effect of $C_{proport}$ the simulation for the average red lettuce population has been extended with another week, as shown in Figure 27.

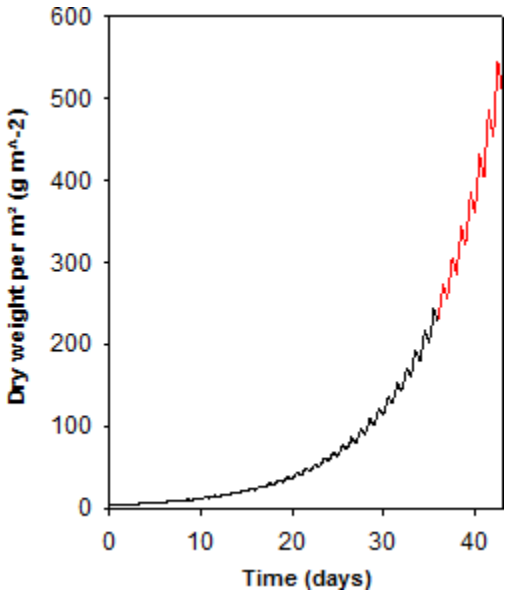

***Figure 27**. An extended version of Figure 27 (b). Model output of Model 1 for the average red lettuce population plotted with an extra 7 simulated days to illustrate the exponential effect of the model on its dry weight.*

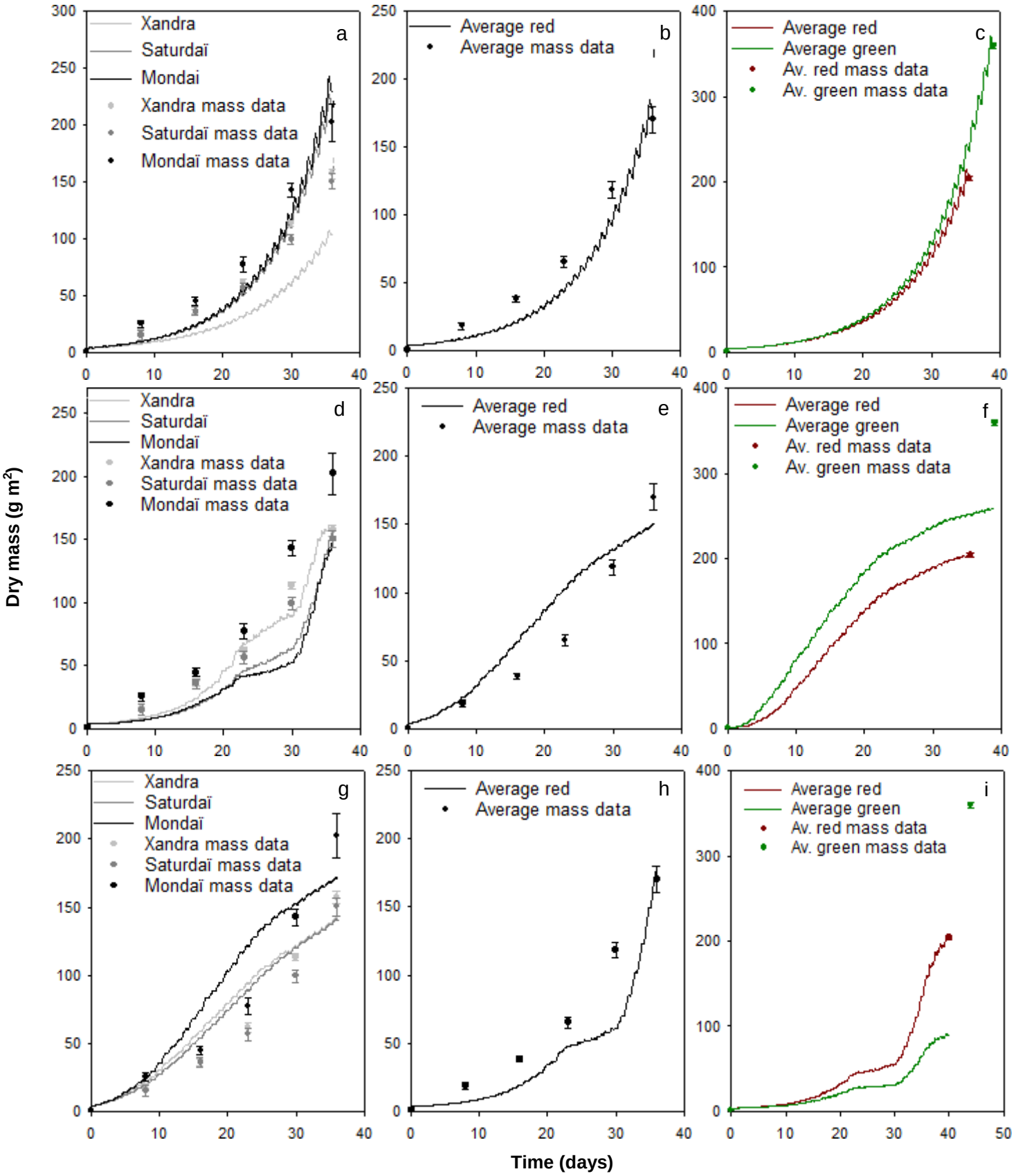

***Figure 28**. The major simulations of all three models. The figures of the first row (a, b and c) represent the model output of model 1, row two (d, e and f) the output of model 2 and row 3 the output of model 3. The first column contains the output of the three red lettuce varieties. The second column contains the output for the average red lettuce population while the third column contains the model output if only mass measurements would be used at plant and harvest date.*

3 Results predictive model using both plant specific and climate factors

3.1 Constants, parameters and calibration boundaries

Values such as C_α, C_{PAR} (PAR fraction of the total radiation) and $C_{raf,rf}$ (transmission coefficient of greenhouse glass) were considered as constants (Table 11). Since they were fixed, they were not included in the calibration.

***Table 11**. Constants used in model 2 with their respective sources.*

Constant	Value	Units	Source
C_α	0.68	-	Van Henten (1994)
C_{PAR}	0.5	-	Van Henten (1994)
$C_{rad,rf}$	0.70	-	(Blindeman *et al.*, 2015)

The parameters were calibrated between the calibration boundaries as presented in Table 12. This calibration occurred within a -20 %, +20 % interval. The values in italics were custom calibration boundaries because of the various reasons mentioned in previous section. C_ε and C_{car3} have slightly lower calibration boundaries to allow unhindered calibration. This adjustment was a decrease from -0.003168 (-20 %) to -0.003432 (-30 %) m s^{-1} for C_{car3}. This was expected to still remain within realistic values. The same was done during the second calibration for the lower limits of C_{resps} and C_{respr} which were lowered to 1e-7 s^{-1} (-70 %) and 7e-6 s^{-1} (-40 %), respectively. To enable a more flexible calibration, C_ε was given very broad calibration boundaries since this is not a parameter with strict physical boundaries. Variables not mentioned above were computed out of previously mentioned constants and inputs.

***Table 12** The parameters used in model 2. The initial values were the parameter values as proposed by their respective sources. These parameters were calibrated within their respective ranges to fit actual harvest data and net photosynthetic production data.*

Parameter	Initial value	Lower boundary	Upper boundary	Units	Source
C_β	0,8	0,64	0,98	-	Sweeney *et al.* (1981), Van Keulen *et al.* (1982)
$C_{resp,s}$	3.47e-7	1.00e-7	4.17e-07	s^{-1}	Van Keulen *et al.* (1982)
$C_{resp,r}$	1.15e-5	9.26e-06	1.36e-05	s^{-1}	Van Keulen *et al.* (1982)
C_τ	0,07	0.056	0.084	-	Lorenz & Wiebe (1980)
$C_{Q10resp}$	2	1,6	2.4	-	Van Henten (1994), Von Caemmerer (2000)
C_k	0,9	*0,3*	*0.95*	-	Goudriaan & Monteith (1990)
C_{lard}	0,075	*0,06*	*0,09*	m^2 kg^{-1}	Lorenz & Wiebe (1980)
C_{car1}	-1,30e-05	-1,60e-05	-1,10-e5	m s^{-1} $°C^{-2}$	Goudriaan *et al.* (1985)
C_{car2}	0,000594	0,000475	0,0007128	m s^{-1} $°C^{-1}$	Goudriaan *et al.* (1985)
C_{car3}	-0,00264	-0,003432	-0,002112	m s^{-1}	Goudriaan *et al.* (1985)
$C_{Q10\Gamma}$	2	1,37	2,2	-	Goudriaan *et al.* (1985)
C_ε	1,70e-05	9e-07	3e-05	g J^{-1}	Goudriaan *et al.* (1985)

3.2 Calibration results

To obtain optimal model parameters, the model was calibrated to dataset 2 in two steps. The first calibration entailed the set 1 parameters needed to calibrate $\Phi_{phot,max}$ to the empiric $P_{n,max}$. The second calibration included all other parameters and used the set 1 parameters as fixed values. The software automatically calculated the object value or the difference between $\Phi_{phot,max}$ and $P_{n,max}$ (Figure 29). It aimed to minimise this value by varying the optimiser variables, as seen in the upper left plot. Eventually, the variable value that resulted in the lowest objective value was chosen as the optimal variable value.

The calibration of the set 1 parameters to fit $\Phi_{phot,max}$ to $P_{n,max}$ yielded the values as presented in Table 13.

***Table 13**. The values of the set 1 parameters after the calibration to the red lettuce dataset (dataset 2).*

Parameter	Calibrated value	Units
C_{lard}	0.0722	$m^2\ kg^{-1}$
C_{car1}	-1. 37e-05	$m\ s^{-1}\ °C^{-2}$
C_{car2}	0. 000610	$m\ s^{-1}\ °C^{-1}$
C_{car3}	-0. 00249	$m\ s^{-1}$
$C_{Q10\Gamma}$	1.89	-
C_{ε}	2.82e-05	$g\ J^{-1}$

This was achieved by evaluating a fictional average lettuce plant which forms the average of a population of red lettuce varieties: Xandra, Saturdaï and Mondaï. This fictional plant had a $P_{n,\max}$ of 15.24 µmol $m^{-2}\ s^{-1}$ or 0.088 g $m^{-2}\ s^{-1}$. The values used for the plant specific parameters were: 0.0882841 mol $m^{-2}\ s^{-1}$ for $Cond$, 9.28972 mol $m^{-2}\ s^{-1}$ for $BLCond$ and 91.2351 µbar for C_{comp25}.

With these values the predicted growth could be calibrated to weekly measured mass growth data. To increase the importance of the final weight during calibration, the final data point was used as a triple overlapping data point. The results for these set 2 parameters could be used for screening other varieties and are presented in Table 14.

***Table 14**. Values of the set 2 parameters after calibration to the red lettuce dataset, dataset 2.*

Parameter	Calibrated value	Units
C_{β}	0.980	-
C_{resps}	2.93e-07	s^{-1}
$C_{resp,r}$	1.18e-05	s^{-1}
C_{τ}	0.0615	-
$C_{Q,10,resp}$	2.19	-
C_{k}	0.548	-

Besides running this simulation for an average population of red lettuce varieties, this was also done for the individual red lettuce varieties Xandra, Saturdaï and Mondaï and for an average population of green lettuce varieties Fairly, Lucrecia and Presteria. For the green lettuce varieties, the upper calibration boundaries had to be increased by 10% for C_{respr}, C_{τ} and C_{resps}.

3.2 Model output

For the individual red lettuce varieties: Xandra, Saturdaï and Mondaï, model simulations were made (Figure 28(d)). The same was done for the average red lettuce population in Figure 28 (e), and for the average red

and average green variety population by only using mass data of the plant and harvest days (Figure 28 (f)). The average red population model has also been applied on Xandra, Saturdaï and Mondaï to evaluate its ability to predict their masses based on the plant specific parameters of these individual varieties (Figure 26 (b)).

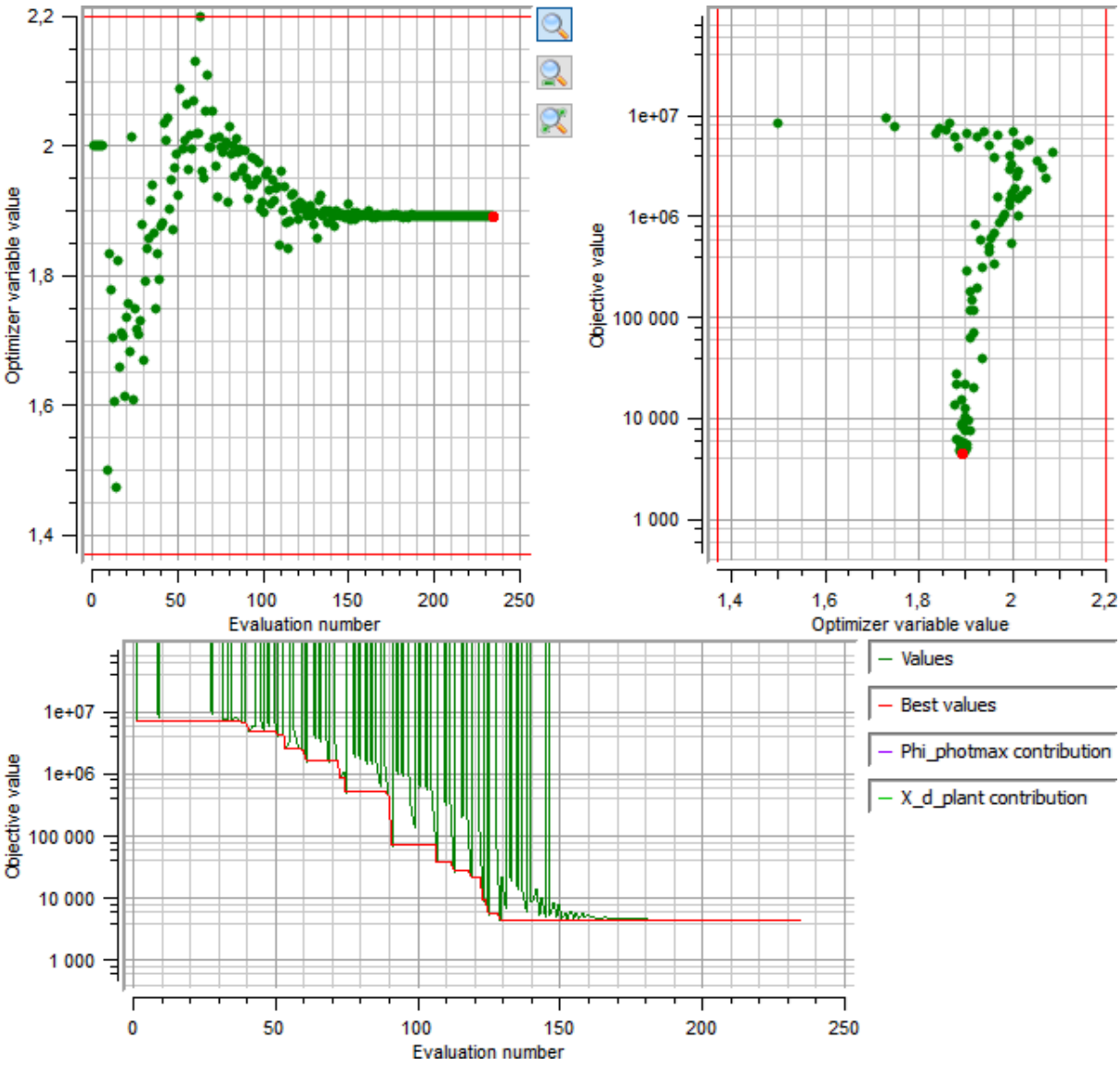

***Figure 29**. An example of the PhytoSim interface during calibration, in this case the calibration of parameter $C_{Q10\Gamma}$. On the upper two graphs, the parameter that was being optimised during the calibration could be seen varied. The lower graph displays the search for the minimal objective value.*

4 Results predictive model using botch climatic and dynamic plant specific parameters

4.1 Calibration

Just as the same structure that was applied for the build-up of the model, also the same two-step calibration procedure and calibration ranges were applied. The first calibration optimised the set 1 parameters while comparing $P_{n,max}$ to $\Phi_{phot,max}$ at maximum CO_2 concentration and incident radiation. The set 1 parameters were: $C_{lard}, C_{car1}, C_{car2}, C_{car3}, C_{Q10\Gamma}$ and C_{ε}. The second calibration compared the predicted weight and the measured weight while optimising the set 2 parameters, being: $C_{\beta}, C_{resp,r}, C_{resp,s}, C_{\tau}, C_{Q10resp}$ and C_k.

Since the values of the plant specific parameters vary through time, a more flexible calibration range was chosen for the parameters that needed to be optimised during calibration one and two. The same boundaries thus used as in Table 10 with the exception of the values mentioned in Table 15. All ranges still remain within physiological realistic values. Values of parameters that couldn't exceed 1.00, such as C_{β} were kept below this value, and values of parameters that cannot be negative, such as C_{τ}, were kept positive. If no multiple values or value ranges for a parameter were found in the literature, a standard +20 % and -20 % were chosen as calibration ranges.

***Table 15**: The parameters used in model 3 with different calibration boundaries than model 2. The values that have been changed are indicated in bold.*

Parameter	Initial value	Lower boundary	Upper boundary	Units	Source
C_{β}	0,8	0,64	0,98	-	Sweeney *et al.* (1981), Van Keulen *et al.* (1982)
$C_{resp,s}$	3.47e-7	1.00e-7	4.17e-07	s^{-1}	Van Keulen *et al.* (1982)
$C_{resp,r}$	1.15e-5	9.26e-06	1.36e-05	s^{-1}	Van Keulen *et al.* (1982)
C_{τ}	0,07	0.056	0.084	-	Lorenz & Wiebe (1980)
$C_{Q10resp}$	2	1,6	**2,2**	-	Van Henten (1994), Von Caemmerer (2000)
C_k	0,9	*0,3*	*0.95*	-	Goudriaan & Monteith (1990)
C_{lard}	0,075	*0,06*	***0,15***	$m^2\ kg^{-1}$	Lorenz & Wiebe (1980)
C_{car1}	-1,30e-05	-1,60e-05	-1,10e-05	$m\ s^{-1}\ °C^{-2}$	Goudriaan *et al.* (1985)
C_{car2}	0,000594	**0.00040**	**0,00085**	$m\ s^{-1}\ °C^{-1}$	Goudriaan *et al.* (1985)
C_{car3}	-0,00264	-0,005	-0,00211	$m\ s^{-1}$	Goudriaan *et al.* (1985)
$C_{Q10\Gamma}$	2	1,37	2,5	-	Goudriaan *et al.* (1985)
C_{ε}	1,70e-05	**3.00e-6**	**3.5e-5**	$g\ J^{-1}$	Goudriaan *et al.* (1985)

The results of this calibration were parameter values for $C_{lard}, C_{car1}, C_{car2}, C_{car3}, C_{Q10\Gamma}$ and C_{ε} as a matrix. Each column contained the 960 parameter values through time per calibration window. The optimal parameter values for the second calibration were given as figures in Figure 30.

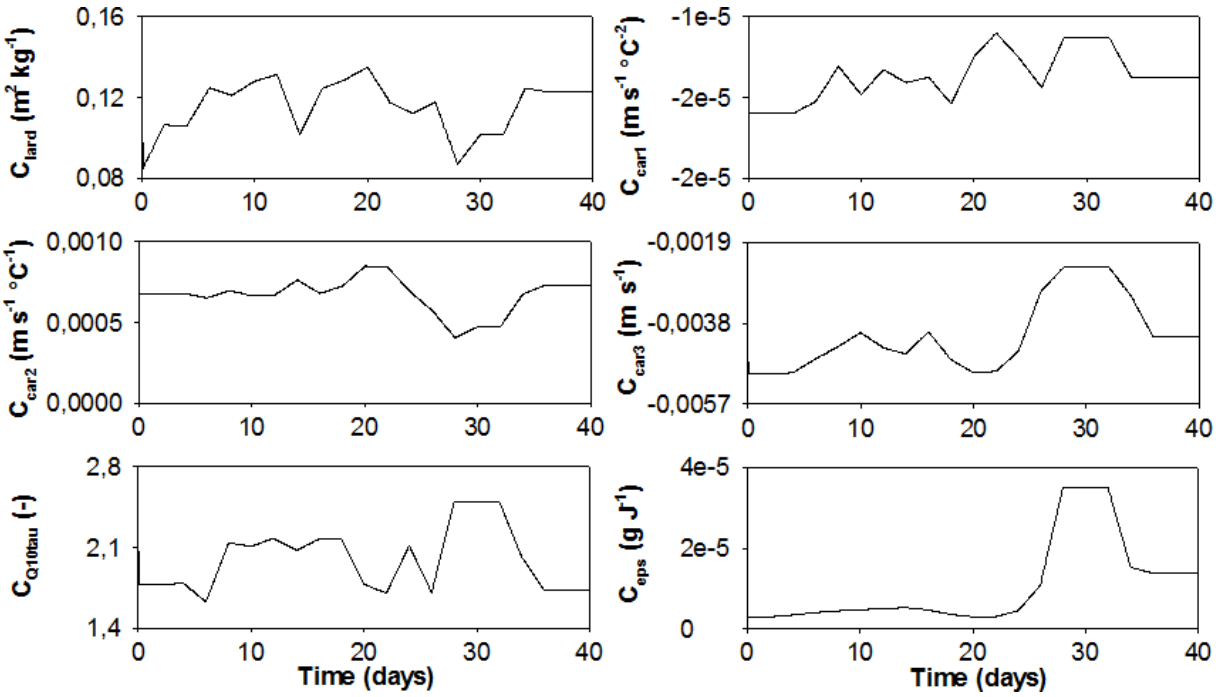

***Figure 30**: The dynamic plant specific parameters that were an output of calibration 1 ($\Phi_{phi,phot,max} = P_{n,max}$), and serves as an input for the same model for calibration 2 ($weight_{measured}$=$weight_{modelled}$).*

4.2 Model output

For the individual red lettuce varieties: Xandra, Saturdaï and Mondaï, model simulations were made (Figure 28 (g)). The same was done for the average red lettuce population in Figure 28 (h), and for the average red and average green variety population by only using mass data of the plant and harvest days (Figure 28 (i)). The average red population model was also applied on Xandra, Saturdaï and Mondaï to evaluate its ability to predict their masses based on the plant specific parameters of these individual varieties (Figure 26 (c)).

Chapter 5
Discussion

1 Introduction

The nine graphs depicted in Figure 27 represent the output of models 1, 2 and 3, each in a different row. Following the graphs from the top to the bottom shows an increase in model complexity. Column one shows the output of the models when describing the growth of the three individual varieties Xandra, Saturdaï and Mondaï. Column two shows the output of the model describing the average red lettuce variety. The third column depicts how the models would be able to work if only one time mass measurements were executed at the end of the grow period. Here, the model was calibrated with two mass data; one at the start and one at the end of the growth period.

Since only a limited dataset is available it is not possible to conduct a real validation. All plant specific data was used to train the model. The aim of building these models is to judge whether or not the growth of these plants can be described with models. The next step can be performing sensitivity analyses and verifications but this was not the aim of the current experimental set-up.

2 Model 1: plant specific parameters based model

The first model is the simplest of all three and is solely based on the carbon balance of the plant. It only has three inputs and is the only model with just one calibration step. It is expected that having such a simple model greatly reduces the amount of error. This can be noticed on Figure 27 (a) when comparing the model output of the individual varieties to the outputs of the other models. Although the predictions are not completely accurate, it does a better job at distinguishing the best variety than model 3. It can also be observed on Figures 26 (b) and 26 (c) that after calibration, model 1 has a closer fit to the measured values. This is not completely possible for model 2 and 3 since they are limited by calibration boundaries for the optimised variables that are ought to be kept at realistic values. This is not exactly an asset of model 1 since this is the direct consequence of including the proportionality constant, $C_{proport}$. This is one of the three optimiser variables that takes account the positive feedback between biomass production and carbohydrate production. A larger plant has more photosynthetic tissue to produce more carbohydrates, which in its turn results in an even larger plant. This parameter does not only include this feedback but also permits a high flexibility for calibrating the predicted mass to the measured mass. A high $C_{proport}$ could have extreme high predicted mass values as a result. Another danger to this model is that growth does not stagnate when using longer growth periods, which would be another cause for extremely high predicted masses. If one would wait another week for harvesting, this model would predict a mass of 510 g m^{-2}, as indicated by the red line

in Figure 26. This corresponds to a lettuce head of 637.5g fresh weight, which is highly unlikely to be correct.

3 Model 2: plant specific and climatic parameters based model

Model 2 also uses climatic inputs. During day 23 and onwards, there was a significantly larger amount of solar radiation than during the first 22 days, as can be seen on Figure 13. This did not have the pronounced effect on the model output as one would think, most probably because of the LED radiation that levels out the DLI to relatively similar levels. The fact that the LED lighting is a significant portion of the total DLI can easily be derived from Figure 18.

In Figure 27 (d) and Figure 27 (e), the model predictions tend to overestimate the dry mass of the plant although it underestimates its final dry mass, which results in a concave growing pattern instead of convex one. The final dry mass data point has a three times larger importance than the other points. Even so, the predictions are not able to calibrate to the relatively high final dry mass. This would imply that the model was restricted by its calibration boundaries or by a shortcoming in the model structure. Further studies with models that contain more physiological relations could explain if the shortcoming is model structure related or not.

The models in the third column do not use intermediary mass data. Being able to predict the growth of lettuce plants with a model that only needed growth data of the plant date and harvest date could make it easier to collect data for setting up these models. It would be good to know for researchers if one measurement is sufficient. In Figure 27 (f) one can remark that if no intermediary dry mass data is used, the concave shape of the curve is more pronounced. There is no intermediary mass data to corrugate the shape of the model predictions during calibration. Even so, the harvest dry mass could be approximated with the model while this is not the case for the average green lettuce population. The cause for this large deviation lies in the fact that there were no measurements for the green plant specific parameters since these were only performed for the red varieties. This indicates that models to describe green lettuce varieties cannot readily use plant specific parameters of red lettuce varieties.

It should also be noted that the mass data used for columns 1 and 2 are different than the mass data of column 3. While the first two columns use mass data measured for the purpose of this thesis, the mass data of column 3 was measured by PSKW. Even with taking into consideration the mass of the soil cube attached to the roots, it is unclear how the harvest mass measured by PSKW is lower than the measured mass of week 5. A possible explanation could be found in a changing fraction of root mass through the growth period of the lettuce plants. The dry mass used in the models exclude the root mass, which is assumed to be 5 % of the total dry mass. A significant deviation of this 5% could explain the discrepancy between the two mass measurements.

4 Model 3: dynamic plant specific and climatic parameters based model

Model 3 uses plant specific parameters that vary through time. This enables the model predictions to attain the more realistic convex shape but seemingly also results in an underestimation of the predicted weights. But unlike model 2, with the same calibration boundaries, model 3 is able to reach the final mass data point in Figure 27 (h).

Also when only using the plant and harvest mass in Figure 27 (i), the mass predictions reach the mass data for the red lettuce varieties. Yet again, the green lettuce variety model which is based on red variety plant specific parameters cannot reach the measured data. This only confirms that one cannot use the plant specific parameters of one variety group to predict the growth of another group.

5 Using the model for vegetable selection

To be able to link these results back to the aim of this thesis, developing models to help the selection of fast growing vegetables to bring to Mars, it could be useful to look at the individual dry weight predictions without calibrating to its mass data. One does not only want to be able to model and describe the growth of a plant, one would also want to predict the mass knowing nothing but certain characteristics of the current plant. When one wants to determine if a vegetable variety will have a higher production than another variety without having to wait the entire growth cycle of the plant, then the mass of these varieties are not known and a general model has to be developed to make predictions of these new varieties. In this case the average red lettuce model has been used as the general model to predict the growth of Xandra, Saturdaï and Mondaï without using their dry mass data for calibration. Only their plant specific parameters were used as inputs.

Having models which enable us to describe the growth of plants under certain conditions, we can evaluate the performances of plants under different climatic conditions. One can virtually vary the CO_2 concentration or temperature to more economical values and examine which plant variety would be the best performer under these new conditions. For example, having a natural high CO_2 concentration in the Martian atmosphere, it is not expensive maintaining a high CO_2 concentration in the Martian grow chamber. Once a plant has been modelled a lot of scenarios can easily be evaluated.

The results as shown in Figure 27 indicate that the models 1 and 2 are able to distinguish the fastest growing plant but still have difficulties at predicting the harvest mass accurately. Model 2 and 3 have the largest deviating model predictions. This is less in model 1 since this deviation could be compensated by the effect of $C_{proport}$. In model 2, deviations could be explained by the fact this simulation output is based on values of $P_{n,max}$, $Cond$ and $BLCond$. The values of these three parameters of only one week were selected to predict the growth of the entire growing period while the values of $P_{n,max}$ tend to vary highly through time. The standard deviation on the $P_{n,max}$ values of Xandra, Saturdaï and Mondaï are 3.46, 5.23, and 5.38 µmol m^{-2} s^{-1}, respectively.

6 Remarks on the measurements

From the measurements of week 3 in dataset 2 and onwards, photosynthetic measurements were performed in the hallway between greenhouse chambers. This was done since measurements on this day (3rd of March 2017) were remarkably low. At the end of an LRC, where P_n is being measured at zero light intensity, P_n values would drop to about -10 µmol CO_2 m^{-2} s^{-1}. The problem would lie in a small leakage from the the atmosphere, where CO_2 levels were as high as 2000 ppm, into the chamber of the LI-6400XT. A higher CO_2 concentration during leakage results in a lower P_n. From this week on measurements were performed in the hallway were CO_2 levels were around 700 ppm. This could also explain why the first photosynthetic measurements resulted in low P_n values while the latest ones gave higher values.

The plants that were measured were significantly smaller than the ones on which no photosynthesis measurements and weighing was performed. This could be a consequence of damage to the roots while removing and placing them back in the gully. The gully has a square shape which narrowly encloses the soil

cube. As the lettuce plants grow older, their root mass becomes larger and protrudes from the cube. Some roots evidently get damaged when removing the cube.

7 Implications

According to these models, an increase in incident radiation would always result in an increased biomass. In practice this is not possible since at higher incident radiation lettuce plants seem to suffer more from tipburn. Tipburn is a breakdown of the edges of the lettuce leaves. It occurs more in the young leaves at the center. It is considered to be a calcium deficiency related disorder although there is still a need for further research. This disorder can cause up to 50 % yield losses in hydroponics (De Swaef et al., 2015). Further understanding of the physiological aspects of tipburn and preventing this disorder could significantly increase the yields of lettuce production under higher incident radiation. This could be a promising prospective in a time where LEDs become more and more economically viable.

8 Suggestions for future measurements

During further development of these models, one can focus on refining the model structure and on validation. Refining the model structure includes determining if there are missing processes for an accurate simulation. This could happen through larger datasets and even more accurate photosynthetic measurements. Several suggestions to have more accurate photosynthetic measurements are:

- Performing measurements outside of the greenhouse or in a space where the CO_2 concentration is close to constant. It has already been discussed that within the greenhouse, CO_2 concentrations can be remarkably high. This could influence the photosynthetic measurements even with a small gas leakage of the leaf chamber. Performing all measurements in the hallway in between the greenhouses could prevent influence of too high CO_2 concentrations. In the future, photosynthetic measurements can be performed in more controlled environment rooms or outside of the confined space of the greenhouse so the CO_2 production of the researchers' bodies can't influence the measurements.
- In the case of leakage using correction factors as presented in the manual of the Li-6400XT as presented by Li-COR, the producer of the photosynthetic measurements machine.
- Using empty chamber measurements. It is more recommended to use the correction factors of the Li6400XT but it is more easily applied in practice. This empty chamber measurement measures the photosynthetic production of the chamber in absence of a leaf. The measured value would be subtracted of the coming values. Although this has been done for dataset 2, it has not been applied for dataset 1 since there was no suspicion of a drift in the photosynthetic productions values back then.

When collecting data of the plants for photosynthetic measurements or weighing, plants should be chosen that are in a specially adapted fitting to allow easy access. This could be a larger opening for the cube so the roots would not touch the metal frame when taking out the plant.

Certain constants and parameters should be closely investigated to determine if they are still realistic for current day technology. Take C_{eps} or the light use efficiency constant for example. Since in these measurements and in practice more and more LED lights are being used, is expected to be higher since LED light is completely useable for the plant, while this cannot be said for sunlight.

Chapter 6
Conclusion & future perspectives

1 Future perspectives

The current models could be further developed by creating a larger dataset with more photosynthetic measurements that allow for a validations of the models. Once the model has been perfected, one can calibrate the model to mass data of each variety and simulate their growth under different climatic conditions. Plotting the growth data versus the CO_2 concentration, temperature or incident radiation can give us the values for ideal growth conditions for each variety. Once these have been found, they can be compared to find out which variety has the largest optimal growth and if these optimal growths are within economically feasible limits.

2 Conclusion

It is possible to approximate the dry mass growth of the plant during its 5 week growing period. The simple model based on the carbon balance, model 1, approaches the measured data well, but tends to predict extreme values at prolonged grow periods and includes a vague parameter $C_{proport}$ which acts as a buffer. Model 2, based on static plant specific parameters and climate data overestimates production during growth but underestimates it at the end. The third model with dynamic plant specific parameters and climatic data tends to underestimate production but can approximate the harvest mass. Dry mass predictions of individual varieties based on a general model can only roughly distinguish faster growing plants from slower growing plants with model 1 and model 2 performing better than model 3.

To conclude, it is possible to simulate the growth of different lettuce varieties using environmental inputs such as temperature, CO_2 concentration and solar and assimilation light although more research should be done to have more accurate simulations. With these models, optimal growth conditions per plant variety can be calculated and the harvest mass that corresponds with these conditions. This harvest biomass and the economic viability of maintaining these climatic conditions in a closed compartment can be used as criteria for the selection of vegetable varieties eligible for Mars.

Bibliography

Ahuja, A. (1997). Integrated M/E Design : Building Systems Engineering (Springer US).

Avercheva, O. V., Berkovich, Y.A., Konovalova, I.O., Radchenko, S.G., Lapach, S.N., Bassarskaya, E.M., Kochetova, G. V., Zhigalova, T. V., Yakovleva, O.S., and Tarakanov, I.G. (2016). Optimizing LED lighting for space plant growth unit: Joint effects of photon flux density, red to white ratios and intermittent light pulses. Life Sci. Sp. Res. *11*, 29–42.

Bakker, J.C. (Jacobus C. (1995). Greenhouse climate control : an integrated approach (Wageningen Pers).

Blindeman, L. (PCS), Schamp, B. (PCS), and Christiaens, A. (PCS) (2015). Zuinig en doordacht belichten, natuurlijk!

von Caemmerer, S. (2000). Biochemical Models of Leaf Photosynthesis.

Chebli, Y., and Geitmann, A. (2011). Gravity Research on Plants: Use of Single-Cell Experimental Models. Front. Plant Sci. *2*, 1–10.

Clarke, M. (2013). The Complete Guide to Building Your Own Greenhouse (Lulu Press, Inc, 2013).

Clawson, J.M., Hoehn, A., and Wheeler, R.M. (2005). Inflatable Transparent Structures for Mars Greenhouse Applications. Engineering.

Cockell, C.S., Bush, T., Bryce, C., Direito, S., Fox-Powell, M., Harrison, J.P., Lammer, H., Landenmark, H., Martin-Torres, J., Nicholson, N., et al. (2016). Habitability: A Review. Astrobiology *16*, 89–117.

Cole, M., and Driscoll, T. (2014). The lighting revolution: If we were experts before, we're novices now. IEEE Trans. Ind. Appl. *50*, 1509–1520.

Cook, E. (2015). Hydroponics Nutrient Film Technique presentation.

Cooper, A. (1970). NFT (Nutrient film Technique). 6–8.

Croswell, K. (2003). Magnificent Mars (Free Press).

Daines, G. (2015). NASA's Journey to Mars.

Danila, E., and Lucache, D.D. (2016). Efficient lighting systems for greenhouses. Proc. 2016 Int. Conf. Expo. Electr. Power Eng. EPE 2016 439–444.

European Space Agency (2004). Europe reclaims a stake in Mars exploration / Mars Express / Space Science / Our Activities / ESA.

European Space Agency (2006). The European Space Exploration Programme Aurora / Exploration / Human Spaceflight / Our Activities / ESA.

European Space Agency (2013). International Space Station Legal Framework.

European Space Agency (2016). The ExoMars programme 2016-2020.

Goudriaan, J., and Monteitht, J.L. (1990). A Mathematical Function for Crop Growth Based on Light Interception and Leaf Area Expansion. Ann. Bot. *66*, 695–701.

Goudriaan, J., van Laar, H.H., van Keulen, H., and Louwerse, W. (1985). Photosynthesis, CO2 and Plant Production. Wheat Growth Model. *86*, 107–122.

Gowda, P.T., Satyareddi, S.A., and Manjunath, S. Crop Growth Modeling: A Review. Res. Rev. J. of Agriculture Allied Sci. *2*, 1–11.

Griffiths, S. (2015). Endemol axes plans for reality TV show that would record life of Mars One explorers | Daily Mail Online.

Grush, L. (2015). Russia announces plans to send humans to the Moon in 2029 - The Verge.

Guteri, F., and Kuyas, F. The Race to Mars | DiscoverMagazine.com.

Haeuplik-Meusburger, S., Paterson, C., Schubert, D., and Zabel, P. (2014). Greenhouses and their humanizing synergies. Acta Astronaut. *96*, 138–150.

Harrington, R. (2016). China plans to reach Mars by 2020 and build a moon base - Business Insider.

Van Henten, E.J. (1994). Validation of a dynamic lettuce growth model for greenhouse climate control. Agric. Syst. *45*, 55–72.

Hoenecke, M.E., Bula, R.J., and Tibbitts, T.W. (1992). Importance of "blue" photon levels for lettuce seedlings grown under red-light-emitting diodes. HortScience *27*, 427–430.

Hoson, T., and Wakabayashi, K. (2015). Phytochemistry Role of the plant cell wall in gravity resistance. Phytochemistry *112*, 84–90.

Howell, E. (2016). How Will a Human Mars Base Work? NASA's Vision in Images.

Javaux, E.J., and Dehant, V. (2010). Habitability: From stars to cells. Astron. Astrophys. Rev. *18*, 383–416.

Jordan, G. (2015). Can Plants Grow with Mars Soil?

Kane, M. Orion update for January 2017 - SpaceFlight Insider.

Van Keulen, H., Penning de Vries, F.W.T., and Drees, E.M. (1982). A summary model for crop growth. Simul. Plant Growth Crop Prod. 87–97.

Kiss, J.Z. (2014). Plant biology in reduced gravity on the Moon and Mars. Plant Biol. *16*, 12–17.

Lamptech (2015). SOX Low Pressure Sodium with IR Coating.

Lehto, K.M., Lehto, H.J., and Kanervo, E.A. (2006). Suitability of different photosynthetic organisms for an extraterrestrial biological life support system. Res. Microbiol. *157*, 69–76.

Lorenz, H.P., and Wiebe, H.J. (1980). Effect of temperature on photosynthesis of lettuce adapted to different light and temperature conditions. Sci. Hortic. (Amsterdam). *13*, 115–123.

Manter, D.K., and Kerrigan, J. (2004). A/Ci curve analysis across a range of woody plant species: Influence of regression analysis parameters and mesophyll conductance. J. Exp. Bot. *55*, 2581–2588.

Mars one (2015a). Roadmap - Mission - Mars One.

Mars one (2015b). Life Support Unit - The Technology - Mars One.

Mars one (2015c). The Technology - Mars One.

Mars one (2015d). Suppliers - About Mars One - Mars One.

Massa, G.D., Kim, H.H., Wheeler, R.M., and Mitchell, C.A. (2008). Plant productivity in response to LED lighting. HortScience *43*, 1951–1956.

Monje, O., Stutte, G.W., Goins, G.D., Porterfield, D.M., and Bingham, G.E. (2003). Farming in space: environmental and biophysical concerns. Adv. Sp. Res. *31*, 151–167.

Morgan, L. (1996). Nutrient Film Technique (NFT) Production of Lettuce.

Nikkei (2016). Japanese engineers working on concrete for lunar base- Nikkei Asian Review.

van Oers, A. (2017). The number of varieties of Romaine lettuce is growing quickly.

Ojha, L., Wilhelm, M.B., Murchie, S.L., Mcewen, A.S., Wray, J.J., Hanley, J., Massé, M., and Chojnacki, M. (2015). Spectral evidence for hydrated salts in recurring slope lineae on Mars. Nat. Geosci. *8*, 1–5.

Ouzounis, T., Rosenqvist, E., and Ottosen, C.-O. (2015). Spectral effects of artificial light on plant physiology and secondary metabolism. Hortscience *50*, 1128–1135.

Di Paola, A., Valentini, R., and Santini, M. (2016). An overview of available crop growth and yield models for studies and assessments in agriculture. J. Sci. Food Agric. *96*, 709–714.

Philips Company (2017). Greenpower LED Toplighting.

Price, H. (2009). Austere Human Missions to Mars.

Proefstation voor de Groeneteelt (2016). LightMan management van licht in bedekte teelten.

Rapp, D. Human missions to Mars : enabling technologies for exploring the red planet.

Read, P.L., Lewis, S.R., and Mulholland, D.P. (2015). The physics of Martian weather and climate: a review. Reports Prog. Phys. *78*, 125901.

Reed, S., and Canadian Electronic Library (2011). Energy-wise landscape design : a new approach for your home and garden (New Society Publishers).

Resh, H.M. (2013). Hobby hydroponics (CRC Press).

Rijk Zwaan Lettuce | Rijk Zwaan UK.

Ryder, E.J. (1999). Lettuce, endive, and chicory (CABI Pub).

Salomez, J., and Hofman, G. (2007). A Soil Temperature/Short-Wave Radiation Growth Model for Butterhead Lettuce Under Protected Cultivation in Flanders. J. Plant Nutr. *30*, 397–410.

Seginer, I., Linker, R., Buwalda, F., van Straten, G., and Bleyaert, P. (2004). The NICOLET lettuce model: A theme with variations. Acta Hortic. *654*.

Seginer, I., Ioslovich, I., and Albright, L. (2005). Strategies for a constant daily light integral in greenhouses. Acta Hortic.

De Swaef, T., Vermeulen, K., Vergote, N., Van Lommel, J., Van Labeke, M.C., Bleyaert, P., and Steppe, K. (2015). Plant sensors help to understand tipburn in lettuce. Acta Hortic. *1099*, 63–70.

Sweeney, D.G., Hand, D.W., Slack, G., and Thornley, J.H.M. (1981). Modelling the growth of winter lettuce. Math. Plant Physiol.

Taylor, F.W. (2010). Planetary atmospheres. Meteorol. Appl. *17*, 393–403.

Tepfer, D., Zalar, A., and Leach, S. (2012). Survival of Plant Seeds, Their UV Screens, and nptII DNA

for 18 Months Outside the International Space Station. Astronbiology *12*.

Wall, M. (2012). Private Manned Mars Mission Gets First Sponsors.

Wall, M. (2013). Radiation on Mars "Manageable" for Manned Mission, Curiosity Rover Reveals.

Williams; Matt (2016). How Bad is the Radiation on Mars? - Universe Today.

Windows to the universe (2010). Mars Global Surveyor : Measures Water Clouds - Windows to the Universe.

Yorio, N.C., Goins, G.D., Kagie, H.R., Wheeler, R.M., and Sager, J.C. (2001). Improving spinach, radish, and lettuce growth under red light-emitting diodes (LEDs) with blue light supplementation. HortScience *36*, 380–383.

Zabel, P., Bamsey, M., Schubert, D., and Tajmar, M. (2016). Review and analysis of over 40 years of space plant growth systems. Life Sci. Sp. Res. *10*, 1–16.

Zachos, E. Growing healthy houseplants : choose the right plant, water wisely, and control pests.

Appendix

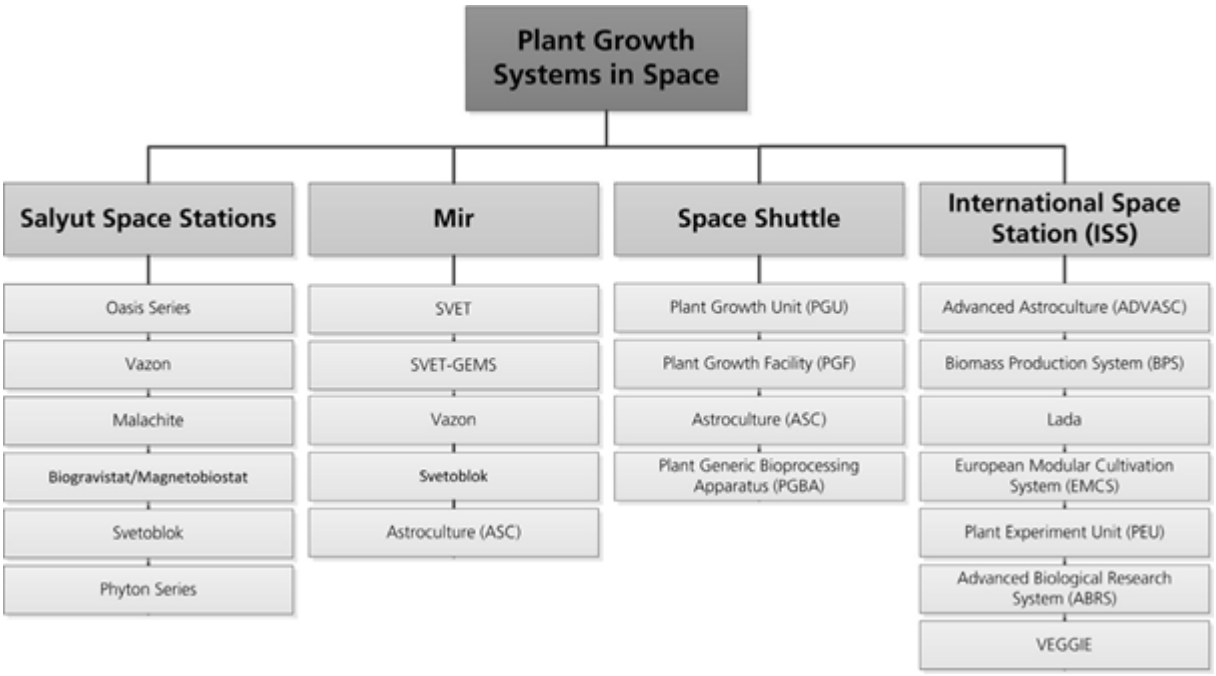

Figure A1. *Overview of the different plant growth chambers in space.*

Table A2. *Detailed information on the illumination systems used in flown plant growth chambers.*

	Lamp type[a]	Light intensity [µmol/(m²*s)]	Additional information
Oasis 1	F	50–68	
Oasis 1M	F	50–68	
Oasis 1AM	F	50–68	
Oasis 1A	F	170–350	Separate illumination and root module allowed adjustments of distance between lamps and plant canopy.
Vazon	no lamps	n.a.	Cabin light was used for plant illumination.
Malachite	type not specified, presumably F	no information	
Biogravistat/ Magnetobiostat	no lamps	n.a.	Closed compartment to study germination and early root development.
Svetoblok	F	no information	
Phyton	no information	no information	First cabin light, later separate illumination system added.
SVET	F	~216 (12.000 lx)	LED (RGB) illumination system tested during an experiment on ground (Ilieva et al., 2010).
SVET-GEMS	F	500	
PGU	F	30–75	
PGF	F	>220	
ASC	LED (RB)[b]	red: 0–450 blue: 0–50	
PGBA	F	>350	
ADVASC	LED (RB)	red: 0–550 blue: 0–70	
BPS	F	50–350	Controllable in 5 µmol/(m²*s) increments.
Lada	F	250	
EMCS	LED (IRW)	no information	
PEU	LED (RB)	110	Red to blue ratio is 3:1.
ABRS	LED (RGBW)	300	
VEGGIE	LED (RGB)	>300	

[a] F=fluorescent lamp; LED=Light Emitting Diode; R=red; B=blue; W=white; G=green; IR=infrared.
[b] First integrated for ASC-2 mission.

Table A3. *Detailed information on the atmosphere management systems used in flown plant growth chambers.*

	Temperature and humidity control	CO_2 control	Trace gas control	Additional information
Oasis 1	no	no	no	Closed vegetation boxes.
Oasis 1M	no	no	no	Closed vegetation boxes.
Oasis 1AM	no	no	no	Closed vegetation boxes.
Oasis 1A	n.a.	n.a.	n.a.	Ventilation fan to remove excessive heat generated by lamps. Plants grew in cabin atmosphere.
Vazon	n.a.	n.a.	n.a.	Plants grew in cabin atmosphere.
Malachite	no	no	no	Closed vegetation box.
Biogravistat/ Magnetobiostat	no	no	no	Closed vegetation box.
Svetoblok	no	no	no	Closed vegetation box. Sterile environment.
Phyton	partly	no	no	Ventilation including bacterial filters.
SVET	partly	no	no	Ventilation fan to remove excessive heat generated by lamps. Oxygen supply to the root module. Environmental condition sensor package including temperature, humidity, substrate moisture.
SVET-GEMS	only temperature	no	no	Two separate air streams (one for plants one for cooling lamps). Large environmental sensor package, including: photosynthesis and transpiration measurements, CO_2 and O_2 sensors, temperature, humidity, substrate moisture.
PGU	only temperature	no	no	Could be equipped with an air exchange system, when sacrificing 1/5 of the cultivation area.
PGF	yes	yes	yes	Ethylene filter.
ASC	yes[a]	yes[b]	yes[c]	Ethylene scrubber unit to fully oxidize ethylene to CO_2 and water.
PGBA	yes	yes	yes	Ventilation with cabin air. Absorption beds to keep CO_2 level within requirements. Same ethylene scrubber technology as ASC.
ADVASC	yes	yes	yes	Same equipment as in ASC.
BPS	yes	yes	yes	Injection of pure CO_2. Ethylene scrubber and particulate filter. Photosynthesis and transpiration measurements.
Lada	yes	no	no	
EMCS	yes	yes	yes	Gas supply unit, pressure control unit, ethylene removal unit.
PEU	yes	yes	no	
ABRS	yes	yes	yes	VOC removal with potassium permanganate ($KMnO_4$).
VEGGIE	only temperature	no	no	Cabin air to control temperature and CO_2 level.

[a] First integrated for ASC-3 mission.
[b] First integrated for ASC-6 mission.

Table A4. *Detailed information on the nutrient delivery systems used in flown plant growth.*

	Nutrient delivery subsystem
Oasis 1	Two compartment system (water and ion exchange resin)
Oasis 1M	Fibrous ion exchange medium
Oasis 1AM	Cloth ion exchange medium
Oasis 1A	Included root zone aeration system
Vazon	Cloth sack filled with ion exchange resin
Malachite	Ion exchange resin, water supply
Biogravistat/ Magnetobiostat	n.a.
Svetoblok	Agar based, later also used other media
Phyton	1.5% agar nutrient medium
SVET	Polyvinyl formal foam surrounded perforated tubing wrapped in a wick within zeolite based substrate enriched with nutrients
SVET-GEMS	Similar to SVET but with additional sensors
PGU	Passive system capable of containing varied substrates/materials
PGF	Passive system capable of containing varied substrates/materials
ASC	Porous tubes in matrix
PGBA	Agar, soil or growth substrate in gas permeable polypropylene bags with option to connect bags to water supply
ADVASC	Porous tubes in matrix
BPS	Porous tubes in matrix
Lada	Perforated tubing wrapped in a wick within a matrix
EMCS	Water reservoir providing water to experiment unique nutrient delivery equipment
PEU	Rock wool fed by integrated water line
ABRS	Experiment specific
VEGGIE	Passive NDS, rooting pillows, manual water and nutrient supply

```
1  // 1. Bruto productie per dag per mol en per gram
   //    ook eigen biomassa in rekening brengend
2  P_bruto = P_max*alpha_c*(PAR-0)/(P_max+alpha_c*(PAR-0))
3  P_bruto_gram=P_bruto*C_naar_gram
4
5  // 2. Dark respiration per dag per mol en per gram
6  //    ook eigen biomassa in rekening brengend
7  R_d = (P_max*alpha_c*(0-I_c)/(P_max+alpha_c*(0-I_c)))
8  R_d_gram = R_d*C_naar_gram
9
10
11 // 3. Data accumumeleren per dag (eerste 12u is dag)
12 if (t%86400 <=43200)
13 {
14 deriv(X_d)=P_bruto_gram*C_proport*X_d+R_d_gram*C_proport*X_d
15 }
16 else
17 // 4. Data accumumeleren per nacht (laatste 12u is nacht)
18 {
19 deriv(X_d)=R_d_gram*C_proport*X_d
20 }
21
22
23 // 10. Droge stof productie per plant
24 X_d_plant = X_d/aantalpervierkantemeter
25
26 // 11. Verse stof productie per plant
27 X_fw = X_d * C_d_naar_fw
28 X_fw_plant = X_fw/aantalpervierkantemeter
```

Figure A2. *The code for model 1 in PhytoSim*

```
// GEBRIUKSWIJZE:-------------------------------------------------------------------------------
// Eerst in excel vorm je Pnmax om tot inleesbare Pnmax in g/m²/s
// Dan calibreer je Phi_phot_max aan deze Pnmax door het varieren van
// alle ondergeschikte parameters. De data van de omgeving wordt cte
// gehouden. Vi = 1000W/m², Xc = 1000ppm en Ti = heersende T (pakt 18°C)

// LI-COR PARAMETERS INVOEGEN-------------------------------------------------------------------
// 1. Pnmax inbrengen
// In excel doen en dan invoeren onder Data Variables

// 2. Geleidbaarheden voor CO2 bepalen uit die van H2O
C_stm_berekend = Cond/(1.6*C_conduct)
C_bnd_berekend = BLCond/(1.37*C_conduct)
C_stm = C_stm_berekend
C_bnd = C_bnd_berekend

// 3. CO2 compensatiepunt
C_comp_20_ubar=C_comp_25*Q_c_comp^(20-25)/10
C_comp_20_g=C_comp_20_ubar*omzet_ubar_naar_gram

// VAN HENTEN MODEL-----------------------------------------------------------------------------
// 1. Relatie droge stof en versgewicht
Y_fw=C_fw*X_d*(1-C_tau)

// 2. Onderhoudsademhaling
Phi_resp=(C_resps*(1-C_tau)+C_respr*C_tau)*X_d*C_Q10resp^((nounit(X_t)-25)/10)

// 3. Invloed temperatuur carboxylatie
Sigma_car = C_car1*X_t^2+C_car2*X_t+C_car3

// 4. Gewas gCO2 conductiviteit + plaffoneren en ondergrens maken
Sigma_CO2 = (C_bnd^-1+C_stm^-1+Sigma_car^-1)^-1

if ( Sigma_CO2 < 0 )
{
 Sigma_CO2 = 0
}
else
{
Sigma_CO2 = Sigma_CO2
}

if ( Sigma_CO2 > 0.00036 )
{
 Sigma_CO2 = 0.00036
}
else
{
Sigma_CO2 = Sigma_CO2
}

// 5. CO2 compensatiepunt Gamma iov Temp
Gamma = C_comp_20_g*C_Q10tau^((nounit(X_t)-20)/10)

// 6. Invloed fotorespiratie op lichtbenutting
eps = C_eps*(X_c-Gamma)/(X_c+2*Gamma)

// 7. Fotosynthese oiv straling, CO2, T, cond
Phi_photmax = (eps*(C_par*C_radrf*V_i+V_LED)*Sigma_CO2*(X_c-Gamma))/(eps*(C_par*C_radrf*V_i+V_LED)+Sigma_CO2*(X_c-Gamma))

// 8. Fotosynthese
Phi_phot = Phi_photmax*(1-exp(-C_k*C_lard*(1-C_tau)*X_d))

// 9. Droge stof productie per m²
deriv(X_d)=C_beta*(C_alpha*Phi_phot-Phi_resp)

// 10. Droge stof productie per plant
//     hierdoor kan ik vergelijken met de grafieken van de literatuur
X_d_plant = X_d/aantalperm2

// 11. Verse stof productie per plant
//     hierdoor kan ik vergelijken met de grafieken van de literatuur
Y_fw_plant = Y_fw/aantalperm2
```

Figure A2. *The code for model 2 in PhytoSim*

```
// GEBRIUKSWIJZE:
// Eerst in excel vorm je Pnmax om tot inleesbare Pnmax in g/m²/s
// Dan calibreer je Phi_phot_max aan deze Pnmax door het varieren van
// alle ondergeschikte parameters. De data van de omgeving wordt cte
// gehouden. Vi = 1000W/m², Xc = 1000ppm en Ti = heersende T (pakt 18°C)


// LI-COR PARAMETERS INVOEGEN
// 1. Pnmax inbrengen
// In excel doen en dan invoeren onder Data Variables

// 2. Geleidbaarheden voor CO2 bepalen uit die van H2O
C_stm_berekend = valueat(Cond,t)/(1.6*C_conduct)
C_bnd_berekend = valueat(BLCond,t)/(1.37*C_conduct)
C_stm = C_stm_berekend
C_bnd = C_bnd_berekend

// 3. CO2 compensatiepunt
C_comp_20_µbar=valueat(C_comp_25,t)*Q_c_comp^(20-25)/10
C_comp_20_g=C_comp_20_µbar*omzet_µbar_naar_gram*20

// 4. Pnmax van µmol/m²/s omzetten naar g/m²/s
Phi_photmax_berekend = MMco2 * vanµmolnaarmol * valueat(Pnmax,t)


// VAN HENTEN MODEL-------------------------------------------------------------------------
// 1. Relatie droge stof en versgewicht
Y_fw=C_fw*X_d*(1-C_tau)

// 2. Onderhoudsademhaling
Phi_resp=(C_resps*(1-C_tau)+C_respr*C_tau)*X_d*C_Q10resp^((nounit(X_t)-25)/10)

// 3. Invloed temperatuur carboxylatie
Sigma_car = valueat(C_car1,t)*X_t^2+valueat(C_car2,t)*X_t+valueat(C_car3,t)

// 4. Gewas gCO2 conductiviteit + plaffoneren en ondergrens maken
Sigma_CO2 = (C_bnd^-1+C_stm^-1+Sigma_car^-1)^-1

if ( Sigma_CO2 < 0 )
{
 Sigma_CO2 = 0
}
else
{
Sigma_CO2 = Sigma_CO2
}

if ( Sigma_CO2 > 0.00036 )
{
 Sigma_CO2 = 0.00036
}
else
{
Sigma_CO2 = Sigma_CO2
}

// 5. CO2 compensatiepunt Gamma iov Temp
Gamma = C_comp_20_g*valueat(C_Q10tau,t)^((nounit(X_t)-20)/10)

// 6. Invloed fotorespiratie op lichtbenutting
eps = valueat(C_eps,t)*(X_c-Gamma)/(X_c+2*Gamma)

// 7. Fotosynthese oiv straling, CO2, T, cond
Phi_photmax = (eps*(C_par*C_radrf*V_i+V_LED)*Sigma_CO2*(X_c-Gamma))/(eps*(C_par*C_radrf*V_i+V_LED)+Sigma_CO2*(X_c-Gamma))

// 8. Fotosynthese
exponent=-C_k*vangnaarkg*valueat(C_lard,t)*(1-C_tau)*X_d
Phi_phot = (Phi_photmax*350)*(1-exp(exponent))

// 9. Droge stof productie per m²
deriv(X_d)=C_beta*(C_alpha*Phi_phot-Phi_resp)

// 10. Droge stof productie per plant
//     hierdoor kan ik vergelijken met de grafieken van de literatuur
X_d_plant = X_d/aantalperm2

// 11. Verse stof productie per plant
//     hierdoor kan ik vergelijken met de grafieken van de literatuur
Y_fw_plant = Y_fw/aantalperm2
```

***Figure A3**. The code for model 2 in PhytoSim*